Applicability of causal dissipative hydrodynamics to relativistic heavy ion collisions

Pasi Huovinen
Department of Physics, University of Virginia, Charlottesville, Virginia 22904, USA and
Physics Department, Purdue University, West Lafayette, Indiana 47907, USA

Denes Molnar
Physics Department, Purdue University, West Lafayette, Indiana 47907, USA and
RIKEN BNL Research Center, Brookhaven National Laboratory, Upton, New York 11973, USA
(Received 19 August 2008; published 28 January 2009)

We utilize nonequilibrium covariant transport theory to determine the region of validity of causal Israel-Stewart (IS) dissipative hydrodynamics and Navier-Stokes (NS) theory for relativistic heavy ion physics applications. A massless ideal gas with $2 \to 2$ interactions is considered in a Bjorken scenario in $0 + 1$ dimension (D) appropriate for the early longitudinal expansion stage of the collision. In the scale-invariant case of a constant shear viscosity to entropy density ratio $\eta/s \approx$ const, we find that IS theory is accurate within 10% in calculating dissipative effects if *initially* the expansion time scale exceeds half the transport mean free path $\tau_0/\lambda_{\mathrm{tr},0} \gtrsim 2$. The same accuracy with NS requires three times larger $\tau_0/\lambda_{\mathrm{tr},0} \gtrsim 6$. For dynamics driven by a constant cross section, on the other hand, about 50% larger $\tau_0/\lambda_{\mathrm{tr},0} \gtrsim 3$ (IS) and 9 (NS) are needed. For typical applications at energies currently available at the BNL Relativistic Heavy Ion Collider (RHIC), i.e., $\sqrt{s_{NN}} \sim$ 100–200 GeV, these limits imply that even the IS approach becomes marginal when $\eta/s \gtrsim 0.15$. In addition, we find that the "naive" approximation to IS theory, which neglects products of gradients and dissipative quantities, has an even smaller range of applicability than Navier-Stokes. We also obtain analytic IS and NS solutions in $0 + 1$D, and present further tests for numerical dissipative hydrodynamics codes in $1 + 1$, $2 + 1$, and $3 + 1$D based on generalized conservation laws.

DOI: 10.1103/PhysRevC.79.014906 PACS number(s): 25.75.−q, 24.10.Nz, 24.10.Lx

I. INTRODUCTION

The realization that shear viscosity is likely nonzero in general [1–3], and therefore the perfect (Euler) fluid paradigm [4–7] of nuclear collisions at the BNL Relativistic Heavy Ion Collider (RHIC) could have significant viscous corrections [8], has fueled great interest in studying dissipative hydrodynamics [9–18]. Causality and stability problems [19] exhibited by standard first-order relativistic Navier-Stokes (NS) hydrodynamics [20,21] steered most effort toward application of the second-order Israel-Stewart (IS) approach [22,23].

However, unlike the NS approach, which comes from a rigorous expansion [24] in small gradients near equilibrium, the IS formulation is *not* a controlled expansion in some small parameter (see Sec. II). Moreover, though causality is restored in a region of hydrodynamic parameters, the stability of IS solutions is not necessarily guaranteed [25]. Therefore it is imperative to test the applicability of the IS approach against a stable, nonequilibrium theory.

In this work we perform such a test utilizing the fully stable and causal covariant transport approach [26–29]. We focus on the special case of $2 \to 2$ transport and a longitudinally boost-invariant system [30] with transverse translational symmetry, i.e., $0 + 1$ dimension (D). Follow-up studies in higher dimensions, such as our earlier comparison between transport and ideal hydrodynamics in $2 + 1$D [8], will be pursued in the future.

A similar study by Gyulassy, Pang, and Zhang [27] compared kinetic theory and Navier-Stokes results. Here we compare kinetic theory to the causal IS solutions. In addition, we provide a series of tests and semianalytic approximations that demonstrate the general behavior of IS solutions, which can be utilized to verify the accuracy of numerical IS solutions.

The paper is structured as follows. We start with reviewing the relationship between hydrodynamics and covariant transport (Sec. II), then proceed to discuss the Israel-Stewart equations (Sec. III). The basic observables studied here are introduced in Sec. IV, while the main results from the hydro-transport comparison are presented in Sec. V, together with implications for heavy ion collisions. Many details are deferred to Appendixes A–D. We highlight here the generalized conservation laws derived in Appendix B and the detailed study of IS and NS solutions in Appendix C utilizing numerical and analytic methods.

II. HYDRODYNAMICS AND COVARIANT TRANSPORT

Hydrodynamics describes a system in terms of a few local, macroscopic variables [20], such as energy density $\varepsilon(x)$, pressure $p(x)$, charge density $n(x)$, and flow velocity $u^\mu(x)$. The equations of motion are energy-momentum and charge conservation

$$\partial_\mu T^{\mu\nu}(x) = 0, \quad \partial_\mu N^\mu(x) = 0, \tag{1}$$

and the equation of state $p(\varepsilon, n)$. *Ideal* (Euler) hydrodynamics assumes local equilibrium, in which case,

$$\begin{aligned} T^{\mu\nu}_{\mathrm{LR,id}} &= \mathrm{diag}(\varepsilon, p, p, p), \\ N^\mu_{\mathrm{LR,id}} &= (n, \mathbf{0}) \quad \left[u^\mu_{\mathrm{LR}} = (1, \mathbf{0})\right], \end{aligned} \tag{2}$$

in the fluid rest frame LR. Extension of the theory with additive corrections *linear* in flow and temperature gradients [20]

$$\delta T^{\mu\nu}_{\mathrm{NS}} = \eta_s\left(\nabla^\mu u^\nu + \nabla^\nu u^\mu - \tfrac{2}{3}\Delta^{\mu\nu}\partial^\alpha u_\alpha\right) + \zeta\,\Delta^{\mu\nu}\partial^\alpha u_\alpha, \tag{3}$$

$$\delta N^{\mu}_{\rm NS} = \kappa_q \left(\frac{nT}{\varepsilon + p}\right)^2 \nabla^{\mu}\left(\frac{\mu}{T}\right) \quad (\Delta^{\mu\nu} \equiv g^{\mu\nu} - u^{\mu}u^{\nu},\ \Delta^{\mu} \equiv \Delta^{\mu\nu}\partial_{\nu}), \tag{4}$$

leads via Eq. (1) to the relativistic NS equations. (We use the Landau frame convention $u_{\mu}\delta T^{\mu\nu} \equiv 0$ throughout this paper, i.e., the flow velocity is chosen such that momentum flow vanishes in the LR frame.) Here $\eta_s(\varepsilon, n)$ and $\zeta(\varepsilon, n)$ are the shear and bulk viscosities, while $\kappa_q(\varepsilon, n)$ is the heat conductivity of the matter. The most notable feature of NS theory relative to the ideal case is dissipation, i.e., entropy production. For consistency, the dissipative corrections (3)–(4) must be small, otherwise nonlinear terms and higher gradients should also be considered.

It is crucial that the above hydrodynamic equations can indeed be obtained from a general nonequilibrium theory, namely, on-shell covariant transport [21,27–29]. For a one-component system, the covariant transport equation reads

$$p^{\mu}\partial_{\mu} f(x, \mathbf{p}) = S(x, \mathbf{p}) + C[f, f](x, \mathbf{p}), \tag{5}$$

where the source term S specifies the initial conditions, and C is the collision term. Throughout this paper, we consider the Boltzmann limit[1] with binary $2 \to 2$ rates

$$C[f, g](x, \mathbf{p}_1) \equiv \int_2 \int_3 \int_4 (f_3 g_4 - f_1 g_2) W_{12\to 34} \delta^4(p_1 + p_2 - p_3 - p_4), \tag{6}$$

where $f_i \equiv f(x, \mathbf{p}_i)$ and $\int_i \equiv \int d^3p_i/(2E_i)$. For dilute systems, f is the phase-space distribution of quasiparticles, while the transition probability $W = (1/\pi)s(s - 4m^2)d\sigma/dt$ is given by the scattering matrix element [21]. Our interest here, on the other hand, is the theory *near its hydrodynamic limit*, $W \to \infty$. In this case, "particles" and "interactions" do not necessarily have to be physical but could simply be mathematical constructs adjusted to reproduce the transport properties of the system near equilibrium [31]. The main advantage of transport theory is its ability to dynamically interpolate between the dilute and opaque limits.

The Euler and Navier-Stokes hydrodynamic equations follow from a rigorous expansion of Eq. (5) in small gradients near local equilibrium

$$f(x, \mathbf{p}) = f_{\rm eq}(x, \mathbf{p})[1 + \phi(x, \mathbf{p})], \quad |\phi| \ll 1, \quad |p^{\mu}\partial_{\mu}\phi| \ll |p^{\mu}\partial_{\mu} f_{\rm eq}|/f_{\rm eq}, \tag{7}$$

and substitution of moments of the solutions

$$N^{\mu}(x) \equiv \int \frac{d^3p}{p_0} p^{\mu}\ f(x, \mathbf{p}),$$

$$T^{\mu\nu}(x) \equiv \int \frac{d^3p}{p_0} p^{\mu}p^{\nu}\ f(x, \mathbf{p}), \tag{8}$$

into Eq. (1). The zeroth order $\phi = 0$ reproduces ideal hydrodynamics. The first-order result is the solution to the linear integral equation

$$p^{\mu}\partial_{\mu} f_{\rm eq}(x, \mathbf{p}) = C[f_{\rm eq}, f_{\rm eq}\phi_{\rm NS}](x, \mathbf{p}) + C[f_{\rm eq}\phi_{\rm NS}, f_{\rm eq}](x, \mathbf{p}) \tag{9}$$

and leads to the NS equations.

Unfortunately, the relativistic Navier-Stokes equations are parabolic and therefore acausal. A solution proposed by Mueller [32] and later extended by Israel and Stewart [22,23] converts the NS equations into relaxation equations for the shear stress $\pi^{\mu\nu}$, bulk pressure Π, and heat flow q^{μ}. The dissipative corrections

$$\delta T^{\mu\nu} \equiv \pi^{\mu\nu} - \Pi\Delta^{\mu\nu}, \quad \delta N^{\mu} \equiv -\frac{n}{\varepsilon + p}q^{\mu} \quad \left(u_{\mu}q^{\mu} = 0, u_{\mu}\pi^{\mu\nu} = u_{\mu}\pi^{\nu\mu} = 0, \pi^{\mu}_{\mu} = 0\right), \tag{10}$$

dynamically relax on microscopic time scales $\tau_{\pi}(\varepsilon, n)$, $\tau_{\Pi}(\varepsilon, n)$, $\tau_q(\varepsilon, n)$ toward values dictated by gradients in flow and temperature. Causality is satisfied in a region of parameter space; however, stability is not guaranteed [25].

More importantly, unlike the Euler and NS equations, the Israel-Stewart approach is not a controlled approximation to the transport theory of Eq. (5). Instead of an expansion in some small parameter, it corresponds to a quadratic ansatz [23,33] for the deviation from local equilibrium

$$\phi_G(x, \mathbf{p}) = D^{\mu}(x)\frac{p_{\mu}}{T} + C^{\mu\nu}(x)\frac{p_{\mu}p_{\nu}}{T^2}, \tag{11}$$

where D^{μ} and $C^{\mu\nu}$ are determined by the local dissipative corrections $\pi^{\mu\nu}$, Π, and q^{μ}.[2] In contrast, the Chapman-Enskog solution (9) contains all orders in momentum. An evident pathology of the quadratic form (11) is that, in general, ϕ_G is not bounded from below, and thus the phase-space density becomes negative at large momenta [cf. Eqs. (7) and (62)]. Furthermore, the two approaches give different results not only for the relaxation times [21,23], e.g.,

$$\tau_{\pi}^{\rm NS} = 0, \quad \tau_{\pi}^{\rm IS} = \frac{3\eta_s}{2p}, \tag{12}$$

but also for the transport coefficients themselves. For an energy-independent isotropic cross section and ultrarelativistic particles ($T \gg m$), the difference is small [21], e.g.,

$$\eta_s^{\rm NS} \approx 0.8436\frac{T}{\sigma_{\rm tr}}, \quad \eta_s^{\rm IS} = \frac{4T}{5\sigma_{\rm tr}}, \tag{13}$$

but can be large for more complicated interactions. Here $\sigma_{\rm tr} \equiv \int d\Omega_{\rm c.m.} \sin^2\theta_{\rm c.m.} d\sigma/d\Omega_{\rm c.m.}$ is the transport cross section (for isotropic, $\sigma_{\rm tr} = 2\sigma_{\rm TOT}/3$).

In the following sections, we analyze IS hydrodynamic solutions analytically and numerically and test the accuracy of the IS approximation via comparison with solutions from full $2 \to 2$ transport theory.

[1] Bose (+) or Fermi (−) statistics can be included in a straightforward manner by substituting $f_1 g_2 \to f_1 g_2(1 \pm \tilde{f}_3)(1 \pm \tilde{g}_4)$ and $f_3 g_4 \to f_3 g_4(1 \pm \tilde{f}_1)(1 \pm \tilde{g}_2)$ in the collision term of Eq. (6) where $\tilde{f} \equiv (1/\gamma)(2\pi)^3 f$ and $\tilde{g} \equiv (1/\gamma)(2\pi)^3 g$ for particles of degeneracy γ. The various hydrodynamic limits can then be derived analogously to the Boltzmann case, if one makes the convenient replacement $\phi \to (1 \pm \tilde{f}_{\rm eq})\phi$ in Eq. (7).

[2] The alternative formulation based on transient thermodynamics [22,23] also lacks a small expansion parameter.

III. ISRAEL-STEWART HYDRODYNAMICS AND BOOST INVARIANCE

A. Israel-Stewart equations

There seems to be some confusion regarding IS theory [22, 23] in the recent literature; therefore, we start with reviewing the key ingredients. The starting point of IS theory is an entropy current that includes terms up to quadratic order in dissipative quantities[3]

$$S^\mu = u^\mu\left[s_{\rm eq} - \frac{1}{2T}(\beta_0\Pi^2 - \beta_1 q_\nu q^\nu + \beta_2\pi^{\lambda\nu}\pi_{\lambda\nu})\right] + \frac{q^\mu}{T}\left(\frac{\mu n}{\varepsilon+p} + \alpha_0\Pi\right) - \frac{\alpha_1 q_\nu \pi^{\nu\mu}}{T} \tag{14}$$

(we follow the Landau frame convention). Here μ is the chemical potential, and $s_{\rm eq}$ is the entropy density in local equilibrium. The coefficients $\{\alpha_i(\varepsilon,n)\}$ and $\{\beta_i(\varepsilon,n)\}$ encode additional matter properties that complement the equation of state the transport coefficients. Most importantly, the parameters $\{\beta_i\}$ control the relaxation times for dissipative quantities:

$$\tau_\Pi = \zeta\beta_0, \quad \tau_q = \kappa_q T\beta_1, \quad \tau_\pi = 2\eta_s\beta_2. \tag{15}$$

The entropy current and relaxation times in NS theory are recovered when all the coefficients are set to zero $\beta_0 = \beta_1 = \beta_2 = 0 = \alpha_0 = \alpha_1$ (but as discussed previously, the IS and NS transport coefficients differ in general).

The requirement of entropy nondecrease ($\partial_\mu S^\mu \geqslant 0$), which IS satisfies via a positive semidefinite[4] quadratic ansatz

$$T\partial_\mu S^\mu = \frac{\Pi^2}{\zeta} - \frac{q_\mu q^\mu}{\kappa_q T} + \frac{\pi_{\mu\nu}\pi^{\mu\nu}}{2\eta_s} \geqslant 0, \tag{16}$$

leads to the identification of the dissipative currents:

$$\Pi = \zeta\left[-\nabla_\mu u^\mu - \frac{1}{2}\Pi T\partial_\mu\left(\frac{\beta_0 u^\mu}{T}\right) - \beta_0 D\Pi + \alpha_0\partial_\mu q^\mu - a_0' q^\mu Du_\mu\right], \tag{17}$$

$$q^\mu = -\kappa_q T\Delta^{\mu\nu}\left[\frac{Tn}{\varepsilon+p}\nabla_\nu\left(\frac{\mu}{T}\right) + \frac{1}{2}q_\nu T\partial_\lambda\left(\frac{\beta_1 u^\lambda}{T}\right) + \beta_1 Dq_\nu + \alpha_0\nabla_\nu\Pi - \alpha_1\partial^\lambda\pi_{\lambda\nu} - a_0\Pi Du_\nu + a_1\pi_{\lambda\nu}Du^\lambda\right], \tag{18}$$

$$\pi^{\mu\nu} = 2\eta_s\left[\nabla^{\langle\mu}u^{\nu\rangle} - \frac{1}{2}\pi^{\mu\nu}T\partial_\lambda\left(\frac{\beta_2 u^\lambda}{T}\right) - \beta_2\langle D\pi^{\mu\nu}\rangle - \alpha_1\nabla^{\langle\mu}q^{\nu\rangle} + a_1' q^{\langle\mu}Du^{\nu\rangle}\right], \tag{19}$$

$$a_i' \equiv \left.\frac{\partial(\alpha_i/T)}{\partial(1/T)}\right|_{\mu/T=\rm const} - a_i. \tag{20}$$

[3]Unlike us here, Israel and Stewart choose $g^{\mu\nu} = {\rm diag}(-1,1,1,1)$, $\Delta^{\mu\nu} = g^{\mu\nu} + u^\mu u^\nu$.

[4]Positive semidefiniteness follows from the general properties $q^\mu q_\mu \leqslant 0$ and $\pi^{\mu\nu}\pi_{\mu\nu} \geqslant 0$.

Here $D \equiv u^\mu\partial_\mu$, and the $\langle\rangle$ brackets denote traceless symmetrization and projection orthogonal to the flow

$$A^{\langle\mu\nu\rangle} \equiv \tfrac{1}{2}\Delta^{\mu\alpha}\Delta^{\nu\beta}(A_{\alpha\beta} + A_{\beta\alpha}) - \tfrac{1}{3}\Delta^{\mu\nu}\Delta_{\alpha\beta}A^{\alpha\beta}. \tag{21}$$

The new matter coefficients $\{a_i(\varepsilon,n)\}$ are needed to describe how contributions from the $q^\mu\Pi$ and $q_\nu\pi^{\mu\nu}$ terms in Eq. (14) are split between the bulk pressure and heat flow, and the heat flow and shear stress evolution equations, respectively (in other words, a whole class of equations of motion generates the same amount of entropy; see Appendix A).

Notice that the time derivatives of heat flow q^μ and shear stress tensor $\pi^{\mu\nu}$ are not expressed *explicitly* in Eqs. (18)–(19); instead, orthogonal projections to the flow velocity vector appear [cf. Eqs. (8a)–(8c) in Ref. [22]]. Reordering the equations explicitly for the time derivatives gives rise to the terms $-u^\mu q_\nu Du^\nu$ and $-(\pi^{\lambda\mu}u^\nu + \pi^{\lambda\nu}u^\mu)Du_\lambda$. There is therefore no need for a kinetic theory treatment [34] to derive these terms. They were missed in Ref. [12], but they are already present in standard IS theory as a trivial consequence of the product rule of differentiation and the orthogonality of the flow velocity and shear stress/heat flow.

As we saw above, the Israel-Stewart procedure only determines the equations of motion up to nonequilibrium terms that do not contribute to entropy production. In kinetic theory, more such terms arise [23] when the vorticity

$$\omega^{\mu\nu} \equiv \tfrac{1}{2}\Delta^{\mu\alpha}\Delta^{\nu\beta}(\partial_\beta u_\alpha - \partial_\alpha u_\beta) \tag{22}$$

is nonzero. Including the vorticity terms, the complete set of evolution equations for the dissipative currents are

$$D\Pi = -\frac{1}{\tau_\Pi}\left(\Pi + \zeta\nabla_\mu u^\mu\right) - \frac{1}{2}\Pi\left(\nabla_\mu u^\mu + D\ln\frac{\beta_0}{T}\right) + \frac{\alpha_0}{\beta_0}\partial_\mu q^\mu - \frac{a_0'}{\beta_0}q^\mu Du_\mu, \tag{23}$$

$$Dq^\mu = -\frac{1}{\tau_q}\left[q^\mu + \kappa_q\frac{T^2 n}{\varepsilon+p}\nabla^\mu\left(\frac{\mu}{T}\right)\right] - u^\mu q_\nu Du^\nu - \frac{1}{2}q^\mu\left(\nabla_\lambda u^\lambda + D\ln\frac{\beta_1}{T}\right) - \omega^{\mu\lambda}q_\lambda - \frac{\alpha_0}{\beta_1}\nabla^\mu\Pi + \frac{\alpha_1}{\beta_1}(\partial_\lambda\pi^{\lambda\mu} + u^\mu\pi^{\lambda\nu}\partial_\lambda u_\nu) + \frac{a_0}{\beta_1}\Pi Du^\mu - \frac{a_1}{\beta_1}\pi^{\lambda\mu}Du_\lambda, \tag{24}$$

$$D\pi^{\mu\nu} = -\frac{1}{\tau_\pi}\left(\pi^{\mu\nu} - 2\eta\nabla^{\langle\mu}u^{\nu\rangle}\right) - (\pi^{\lambda\mu}u^\nu + \pi^{\lambda\nu}u^\mu)Du_\lambda - \frac{1}{2}\pi^{\mu\nu}\left(\nabla_\lambda u^\lambda + D\ln\frac{\beta_2}{T}\right) - 2\pi_\lambda^{\langle\mu}\omega^{\nu\rangle\lambda} - \frac{\alpha_1}{\beta_2}\nabla^{\langle\mu}q^{\nu\rangle} + \frac{a_1'}{\beta_2}q^{\langle\mu}Du^{\nu\rangle}. \tag{25}$$

We will refer to these equations as "complete IS." If we ignore their tensorial structure, the equations have the general form

$$\dot X = -\frac{1}{\tau_X}(X - X_{\rm NS}) + X\,Y_X + Z_X \tag{26}$$

for each dissipative quantity X, where $X_{\rm NS}$ is the value of X in NS theory and Y_X, Z_X are given by the ideal hydrodynamic fields and dissipative quantities other than X. Therefore, IS theory describes relaxation toward Navier-Stokes on a

characteristic time τ_X, provided $|Y_X|\tau_X \ll 1$ and $|Z_X|\tau_X \ll |X_{\rm NS}|$. If Y_X and/or Z_X are not small, the effective relaxation times in IS theory differ from τ_X; moreover, the relaxation of dissipative quantities is no longer toward their NS values. This has been discussed in Ref. [12], which, however, argued for dropping all $XY_X + Z_X$ terms for the very same reason.

In the last step of their derivation, Israel and Stewart neglect the terms with the factor 1/2 (this gives the equivalent to [23]), because they expect to study astrophysical systems with small gradients $|\partial^\mu u^\nu + \partial^\nu u^\mu|/T \ll 1$, $|\partial^\mu \varepsilon|/(T\varepsilon) \ll 1$, $|\partial^\mu n|/(Tn) \ll 1$, near a global (possibly rotating) equilibrium state. The neglected terms are then products of small gradients and the dissipative quantities. We will refer to this approximation as "naive IS."[5]

In heavy ion physics applications, on the other hand, gradients $\partial^\mu u^\nu/T$, $|\partial^\mu \varepsilon|/(T\varepsilon)$, and $|\partial^\mu n|/(Tn)$ at early times $\tau \sim 1$ fm are large $\sim\mathcal{O}(1)$, and therefore cannot be ignored. Nevertheless, hydrodynamics may still be applicable, provided the viscosities are unusually small, i.e., $\eta_s/s_{\rm eq} \sim 0.1$, $\zeta/s_{\rm eq} \sim 0.1$, where $s_{\rm eq}$ is the entropy density in local equilibrium. In this case, dissipative effects are still moderate, for example, the pressure corrections from NS theory [Eq. (3)] are

$$\frac{\delta T^{\mu\nu}_{\rm NS}}{p} \approx \left(2\frac{\eta_s}{s_{\rm eq}}\frac{\nabla^{\langle\mu}u^{\nu\rangle}}{T} + \frac{\zeta}{s_{\rm eq}}\frac{\nabla_\alpha u^\alpha}{T}\right)\frac{\varepsilon+p}{p} \sim \mathcal{O}\left(\frac{8\eta_s}{s_{\rm eq}}, \frac{4\zeta}{s_{\rm eq}}\right) \tag{27}$$

Heat flow effects can also be estimated based on Eq. (4):

$$\frac{\delta N^\mu_{\rm NS}}{n} \approx \frac{\kappa_q T}{s_{\rm eq}}\frac{n}{s_{\rm eq}}\frac{\nabla^\mu(\mu/T)}{T}. \tag{28}$$

For RHIC energies and above, at midrapidity, the correction is rather small even for large κ_q because the baryon density and therefore μ_B/T is very low. For example, in a recent ideal fluid calculation at RHIC energy [36], these ratios were $n_B/s \approx 2.2\times10^{-3}$ and $\mu_B/T \approx 0.2$ in order to reproduce the observed net baryon spectra. These choices are also supported by thermal model analyses of particle ratios which lead to $\mu_B/T \approx 0.17$ [37].

B. Viscous equations of motion for longitudinally boost-invariant 0 + 1D dynamics

At this point, we specialize the equations of motion to a viscous, longitudinally boost-invariant[6] system with transverse translation invariance and vanishing bulk viscosity:

$$\dot{n} + \frac{n}{\tau} = 0 \quad\Leftrightarrow\quad n(\tau) = \frac{\tau_0 n(\tau_0)}{\tau}, \tag{29}$$

$$\dot{\varepsilon} + \frac{\varepsilon+p}{\tau} = -\frac{\pi_L}{\tau}, \tag{30}$$

$$\tau_\pi\dot{\pi}_L + \pi_L\left[1 + \frac{\tau_\pi}{2\tau} + \frac{\eta_s T}{2}\left(\frac{\dot{\tau}_\pi}{\eta_s T}\right)\right] = -\frac{4\eta_s}{3\tau}, \tag{31}$$

$$\pi_T = -\frac{\pi_L}{2}. \tag{32}$$

This special case is well known in the literature [9,34,38] as a useful approximation to the early longitudinal expansion stage of a heavy ion collision for observables near midrapidity $\eta \approx 0$. Here $\tau \equiv \sqrt{t^2 - z^2}$ is the Bjorken proper time, and the 'dot' denotes $d/d\tau$. π_L and π_T are the viscous corrections to the longitudinal and transverse pressure, i.e., the π_{zz} and $\pi_{xx} = \pi_{yy}$ components of the shear stress tensor evaluated in the local rest frame,[7] respectively. All the other components of the stress tensor are zero due to symmetry. There is no equation for heat flow, because the symmetries of the system—longitudinal boost-invariance, axial symmetry in the transverse plane, and $\eta \to -\eta$ reflection symmetry—force the heat flow to be zero everywhere. We have chosen to ignore bulk viscosity, since shear viscosity is expected to dominate at RHIC. In the following, we also concentrate on a system of massless particles, where bulk viscosity is zero in general. It is worth noticing that these equations are identical in both Eckart and Landau frames; but in less restricted systems where heat flow is nonzero, Eckart and Landau frames differ.

To simplify the discussion and facilitate comparison with transport results, from here on we concentrate on a system of massless particles with only elastic $2 \to 2$ interactions. Particle number is then conserved, and the equation of state is

$$\varepsilon = 3p, \quad T = \frac{p}{n}. \tag{33}$$

Now the density equation decouples entirely, and we end up with two coupled equations for the equilibrium pressure and the viscous correction π_L. The shear stress relaxation time of Eq. (12) and the shear viscosity of Eq. (13) can be recast with the *transport* mean free path $\lambda_{\rm tr} \equiv 1/(n\sigma_{\rm tr})$ as

$$\eta_s = CnT\lambda_{\rm tr}, \quad \tau_\pi = \frac{3C}{2}\lambda_{\rm tr}, \quad C \approx \frac{4}{5}, \tag{34}$$

and Eqs. (30) and (31) can then be written as

$$\dot{p} + \frac{4p}{3\tau} = -\frac{\pi_L}{3\tau}, \tag{35}$$

$$\dot{\pi}_L + \frac{\pi_L}{\tau}\left(\frac{2\kappa(\tau)}{3} + \frac{4}{3} + \frac{\pi_L}{3p}\right) = -\frac{8p}{9\tau}, \tag{36}$$

where

$$\kappa(\tau) \equiv \frac{K(\tau)}{C} = \frac{nT\tau}{\eta_s}, \quad K(\tau) \equiv \frac{\tau}{\lambda_{\rm tr}(\tau)}. \tag{37}$$

The ratio of expansion and scattering time scales K controls how well ideal and/or dissipative hydrodynamics applies. This is essentially the *inverse* of the ratio of shear stress relaxation time to hydrodynamic time scales $\tau_\pi/\tau = 3/(2\kappa)$. K is also a generalization of the inverse Knudsen number L/λ, since the shortest spatial length scale is given by gradients in the longitudinal direction $L \sim 1/(\partial_z u_z) \sim \tau$. It is also a measure

[5] Note that in Ref. [35], the equivalent sets of equations are called "full IS" and "simplified IS."

[6] By a boost-invariant system we mean a system that obeys the scaling flow, $v = (0, 0, z/t)$, where all scalar quantities are independent of coordinate rapidity $\eta \equiv (1/2)\ln[(t+z)/(t-z)]$, and where all vector and tensor quantities can be obtained from their values at $\eta = 0$ by an appropriate Lorentz boost.

[7] That is, in the often employed curvilinear τ-η-x-y coordinates, we have $\pi_{\eta\eta} = \tau^2\pi_L$.

of the shear viscosity to entropy density ratio, because for a system in chemical equilibrium, $s_{\rm eq} = 4n$ and thus

$$\frac{\eta_s}{s_{\rm eq}} = \frac{T\tau}{4\kappa}. \tag{38}$$

(See Sec. V E for the general case.)

Similar treatment to relativistic NS theory leads to

$$\pi_L = -\frac{4\eta_s}{3\tau} = -\frac{4p}{3\kappa} \tag{39}$$

and the equation of motion

$$\dot{p} + \frac{4p}{3\tau} = \frac{4}{9\kappa(\tau)}\frac{p}{\tau}. \tag{40}$$

As discussed in the previous section, the viscosities in NS and IS theories differ; therefore, κ in Eq. (40) is not identical to the one in Eq. (36). We will ignore the difference, because in our case it is only ≈5%.

Finally, we note that in the "naive" Israel-Stewart approximation, Eq. (36) changes to

$$\dot{\pi}_L + \frac{2\kappa(\tau)\pi_L}{3\tau} = -\frac{8p}{9\tau}. \tag{41}$$

IV. BASIC OBSERVABLES

Here we introduce the basic observables investigated in this study and discuss their evolution based on the analytic IS and NS solutions of Appendix C. It is important to emphasize that our observations will hold only during the longitudinal expansion stage of heavy ion collisions. After some time $\tau \sim R/c_s$, transverse expansion sets in, and hydrodynamics, whether IS or NS, eventually breaks down, because for expansion in three dimensions, $\lambda_{\rm tr} \sim \tau^3/\sigma$, i.e., $\kappa \sim \sigma/\tau^2 \to 0$ in the hadronic world where cross sections are bounded. It is interesting to note that $\eta_s/s_{\rm eq} \approx$ const would not decouple even for a three-dimensional expansion (because in that case $T \propto 1/\tau$, and thus $\lambda_{\rm tr} \propto \eta/p \propto \tau$, while $\tau_{\rm exp} \equiv 1/(\partial_\mu u^\mu) \propto \tau$, i.e., $\kappa \sim$ const).

Throughout this section and the rest of the paper, the subscript 0 refers to the value of quantities at the initial time τ_0 [e.g., $A_0 \equiv A(\tau_0)$]. The most important parameters in the problem are the initial inverse Knudsen number K_0, or the corresponding κ_0, and the initial shear stress to pressure ratio $\xi_0 \equiv \pi_{L,0}/p_0$.

A. Pressure anisotropy

The magnitude of dissipative corrections can be quantified through the ratio of viscous longitudinal shear and equilibrium pressure

$$\xi \equiv \frac{\pi_L}{p}. \tag{42}$$

A suitable equivalent measure is the pressure anisotropy coefficient

$$R_p \equiv \frac{p_L}{p_T} = \frac{1+\xi}{1-\xi/2}, \tag{43}$$

which is the ratio of the transverse and longitudinal pressures $p_T \equiv p - \pi_L/2$ and $p_L \equiv p + \pi_L$. In the ideal hydrodynamic limit, the anisotropy is unity, $R_p \to 1$.

The time evolution of the anisotropy coefficient is given by the equations of motion (35) and (36):

$$\dot{R}_p = -\frac{4}{3\tau}\frac{4+3\kappa\xi}{(2-\xi)^2}. \tag{44}$$

Thus, in IS theory the pressure anisotropy is a constant of motion when the viscous stress is equal to its NS value [Eq. (39)], or at asymptotically late times $\tau \to \infty$. In contrast, from NS theory,

$$R_p^{\rm NS} = \frac{3\kappa - 4}{3\kappa + 2}, \tag{45}$$

which is only constant for $\kappa(\tau) =$ const (constant cross section), or in the ideal hydrodynamic limit $\kappa \to \infty$ (in which case, $R_p \to 1$). From the above, it also follows that in the special case of our boost-invariant scenario, if the cross section is constant and the shear stress starts from its NS value, then NS and IS theory *coincide*.

B. Longitudinal work

Dissipation also affects the evolution of the equilibrium (or average) pressure. From Eq. (35), for ideal hydrodynamic evolution, the pressure drops as $p(\tau) \propto \tau^{-4/3}$ because of longitudinal work. In the viscous case, the work done by the system is smaller, because the viscous correction to the longitudinal pressure is usually negative $\pi_L < 0$. Therefore, pressure decreases slower than in ideal hydrodynamics, and deviations from the ideal evolution, such as the ratio

$$\frac{p(\tau)}{p_{\rm ideal}(\tau)} \equiv \frac{T(\tau)}{T_{\rm ideal}} \quad \text{(for conserved particle number)}, \tag{46}$$

can be used to quantify dissipative effects.

Studies in the past [27,28] have analyzed a closely related quantity, the transverse energy per unit rapidity, $dE_T/d\eta$. This is simply a combination of the pressure anisotropy and deviation from ideal pressure

$$\begin{aligned}\frac{dE_T}{d\eta} &= \frac{3\pi T}{4}\frac{dN}{d\eta}\left(1 - \frac{5}{16}\xi\right) \\ &= \frac{3\pi T_0}{4}\frac{dN}{d\eta}\left(\frac{\tau_0}{\tau}\right)^{-1/3}\frac{p(\tau)}{p_{\rm ideal}(\tau)}\frac{3[7+R_p(\tau)]}{8[2+R_p(\tau)]}\end{aligned} \tag{47}$$

provided the quadratic ansatz (11) is applicable (see Appendix D1).

We can make a few generic observations based on the analytic IS and NS results of Eqs. (C4), (C8), (C21), (C22), and (C29) from Appendix C. For a constant cross section, $p/p_{\rm ideal}$ grows without bound, dissipative corrections keep accumulating forever. The influence of the initial shear stress, or equivalently shear stress to pressure ratio $\xi_0 \equiv \xi(\tau_0)$, is of $\mathcal{O}(\xi_0/\kappa_0)$ and thus vanishes in the large κ_0 limit. At late times $\tau \gg \tau_0$, for $K_0 \gtrsim 2$ and not too large initial shear stress to pressure ratio $|\xi_0| \ll 2\kappa_0$,

$$\begin{aligned}\left(\frac{p}{p_{\rm ideal}}\right)_{\sigma=\rm const} &\approx N\left(\frac{\tau}{\tau_0}\right)^{\beta}, \quad \beta \approx \frac{4}{9\kappa_0}\left(1 - \frac{2}{3\kappa_0^2}\right), \\ N &\approx 1 - \frac{2}{3\kappa_0^2} + \frac{4}{3\kappa_0^4} - \frac{\xi_0}{2\kappa_0},\end{aligned} \tag{48}$$

i.e., for $\tau \approx 10\tau_0$ and $K_0 = 2$ the accumulated pressure increase is $p/p_{\rm ideal} \approx 1.3$, while $p/p_{\rm ideal} \approx 1.15$ if $K_0 = 5$. For a scale-invariant system with $\eta_s/s_{\rm eq} \approx$ const, on the other hand, dissipative effects are more moderate for the same K_0 and at late times approach a finite upper bound

$$\left(\frac{p}{p_{\rm ideal}}\right)_{\eta/s\approx{\rm const}} \approx \left[1 - \frac{2}{3\kappa_0}\left(\frac{\tau_0}{\tau}\right)^{2/3}\right]\left(1 + \frac{2}{3\kappa_0} - \frac{\xi_0}{2\kappa_0}\right) \to 1 + \frac{2}{3\kappa_0} - \frac{\xi_0}{2\kappa_0}. \quad (49)$$

This is because scale-invariant systems turn more and more ideal hydrodynamically as they evolve (as long as their expansion is only longitudinal). For the same $K_0 = 2$ and 5 with $\xi_0 \approx 0$, the bounds are modest: $p/p_{\rm ideal} \lesssim 1.25$ and $\lesssim 1.1$, respectively.

C. Entropy

Another quantitative measure of the importance of dissipative effects is entropy production. Here we consider an ultrarelativistic system [thus $\Pi = 0$ and $\beta_2 = 3/(4p)$], with $2 \to 2$ interactions, 1D Bjorken boost invariance, and transverse translational, axial, and $\eta \to -\eta$ reflectional symmetries (imply $q^\mu = 0$). Therefore, the entropy current of Eq. (14) simplifies to

$$S^\mu = \bar{s}u^\mu, \quad \bar{s} = s_{\rm eq} - \frac{9\pi_L^2}{16pT}, \quad (50)$$

where

$$s_{\rm eq} = n(4 - \chi), \quad \chi \equiv \ln\frac{n}{n_{\rm eq}(T)} = \frac{\mu}{T}, \quad (51)$$

and

$$n_{\rm eq}(T) = \frac{g}{\pi^2}T^3 \quad (52)$$

is the particle density in chemical equilibrium at temperature T for massless particles of degeneracy g in the Boltzmann limit. Dissipative contributions in the entropy density $\bar{s}$ are *negative*, in accordance with the fundamental principle of maximal entropy in equilibrium.

The equations of motion (35) and (36) imply an entropy production rate of

$$\partial_\mu S^\mu = \frac{1}{\tau}\partial_\tau(\tau\bar{s}) = \frac{3\kappa n}{4\tau}\xi^2 \geqslant 0. \quad (53)$$

Equivalently, the entropy per unit rapidity

$$\frac{dS}{d\eta} \equiv \tau A_T \bar{s} \quad (54)$$

never decreases, that is,

$$\partial_\tau\left(\frac{dS}{d\eta}\right) = \frac{3\kappa}{4\tau}\frac{dN}{d\eta}\xi^2 \geqslant 0. \quad (55)$$

Here A_T is the transverse area of the system, and in the last step we substituted the rapidity density $dN/d\eta = \tau A_T n$. Equation (54) is a special case of a *generalized conservation law* [Eq. (B7)] applied to the entropy current S^μ, that is,

$$\tau\int dx_T^2\,\partial_\mu S^\mu = \partial_\tau\left(\tau\int dx_T^2\,S_0^{\rm LR}\right) - \partial_\eta\int dx_T^2\,S_3^{\rm LR}. \quad (56)$$

Analogous relations can be obtained for the energy, momentum, and charge density. In 0 + 1D these are quite trivial; they, respectively, reproduce Eq. (35), give identically zero, and yield $dN/d\eta =$ const. In higher dimensions, however, the generalized conservation laws present important constraints that *any* solution must satisfy at *all* times; therefore, they are ideal for testing the accuracy of numerical solutions at each time step (see Appendix B).

Only the complete set of IS equations gives the correct rate of entropy production. The naive approximation does not guarantee a monotonically increasing entropy

$$(\partial_\mu S^\mu)^{\text{naive IS}} = \frac{3\kappa n}{4\tau}\xi^2\left(1 - \frac{\xi + 4}{2\kappa}\right) \quad (57)$$

unless κ is sufficiently large; and, away from equilibrium, it underpredicts for a given ξ the entropy production rate[8] (since $\xi < -1$ is unphysical). In contrast, the second law of thermodynamics does hold for Navier-Stokes:

$$(\partial_\mu S^\mu)^{\rm NS} = \frac{3\kappa n}{4\tau}\xi_{\rm NS}^2 \geqslant 0. \quad (58)$$

The NS result is the same as Eq. (53) but with the shear stress restricted to its NS value. We note that in IS theory, the naive entropy per unit rapidity, defined using the *equilibrium* entropy density

$$\frac{dS'}{d\eta} = s_{\rm eq}\tau A_T \quad (59)$$

does *not* increase monotonically. Rather, it increases (decreases) for negative (positive) π_L.

Based on the analytic IS and NS results in Appendix C, we can outline general expectations for the entropy evolution. For a constant cross section by late times $\tau \gg \tau_0$, the entropy increase relative to the initial entropy is logarithmic with time, i.e.,

$$\left[\frac{(dS/d\eta)}{(dS/d\eta)_0}\right]_{\sigma={\rm const}} - 1 \approx \frac{1}{4 - \chi_0}\left(3\ln\frac{p}{p_{\rm ideal}} - \frac{9\xi^2}{16}\right) \approx \frac{1}{4 - \chi_0}\left(3\beta\ln\frac{\tau}{\tau_0} - \frac{3}{\kappa_0^2} + \frac{16}{3\kappa_0^4} - \frac{3\xi_0}{2\kappa_0}\right), \quad (60)$$

where we considered initial conditions not too far from local equilibrium. For example, by $\tau \approx 10\tau_0$ with $K_0 = 2$ and chemical equilibrium initial conditions, ≈20% entropy is produced, while ≈10% with $K_0 = 5$. For a scale-invariant system with

[8] This, however, does *not* imply that the naive IS equations always underpredict the *total* integrated entropy change over a finite time interval. The time evolution of $\xi(\tau)$ in the naive approach differs in general from that in the complete theory.

$\eta_s/s_{\rm eq} = {\rm const}$, on the other hand, entropy production is slower for the same K_0 and saturates at late times, i.e.,

$$\left[\frac{(dS/d\eta)}{(dS/d\eta)_0}\right]_{\eta/s\approx{\rm const}} - 1 \approx \frac{1}{4-\chi_0}\frac{2}{\kappa_0}\left[1-\left(\frac{\tau_0}{\tau}\right)^{2/3}-\frac{3\xi_0}{4}\right] \to \frac{1}{4-\chi_0}\frac{2}{\kappa_0}\left(1-\frac{3\xi_0}{4}\right) = \frac{2}{T_0\tau_0}\frac{\eta_s}{s_{\rm eq}}\left(1-\frac{3\xi_0}{4}\right). \quad (61)$$

For the same $K_0 = 2$ and 5 (and $\xi_0 \approx 0$), the entropy increase by $\tau = 10\tau_0$ is smaller, ≈15% and ≈6%, respectively. Based on this simple analytic formula for entropy production, we also confirm the results of Ref. [38], which considered IS hydrodynamics with a unique initial condition $\xi_0 \approx -16/(9T_0\tau_0) \times \eta_s/s_{\rm eq}$, where $T_0 \approx 0.39$ GeV $\times$ (0.14 fm/τ_0)$^{1/3}$ and τ_0 was varied between 0.5 and 1.5 fm.

V. REGION OF VALIDITY FOR DISSIPATIVE HYDRODYNAMICS

Here we determine the region of validity of dissipative hydrodynamics by comparing it with full nonequilibrium two-body transport theory [26–29]. We consider two scenarios: scenario I with a constant cross section, which is least favorable for hydrodynamics; and scenario II with a growing $\sigma \propto \tau^{2/3}$, which is the most optimistic for applicability of hydrodynamics and is very close to $\eta_s/s_{\rm eq} = {\rm const}$, as we show in Appendix C. In the same appendix, we also study a scenario with $\sigma \propto 1/T^2$, which turns out to be close to scenario II but with stronger dissipative effects, and we discuss analytic NS and (approximate) IS solutions.

Because of scalings of the equations of motion, the results presented here are rather general. Equations (35) and (36) are invariant under rescaling of time, and/or joint rescaling of the pressures p and π_L, provided the dimensionless κ depends only on p, π_L, τ/τ_0, and no additional scales (all solutions studied here satisfy this condition). The same scalings are exhibited by the transport theory [28]. For a physically reasonable $p_0 > 0$, it is therefore convenient to consider dimensionless pressure variables $\tilde{p}(\tau) \equiv p(\tau)/p_0$ and $\pi_L(\tau)/p_0$, for which the solutions only depend on $\tilde{\tau} \equiv \tau/\tau_0$, $\kappa_0 \equiv K_0/C$, and the initial condition $\xi_0 \equiv \pi_{L,0}/p_0$.

Unless stated otherwise, we initialize the transport based on the quadratic form in Eq. (11). In our case of an ultrarelativistic system ($\varepsilon = 3p$) in the Boltzmann limit with vanishing bulk pressure and heat flow

$$D^\mu = 0, \quad C^{\mu\nu} = \frac{\pi^{\mu\nu}}{8p} \Rightarrow \phi_G(\eta=0,\mathbf{p}) = \frac{\xi}{16}\frac{2p_z^2 - p_\perp^2}{T^2}, \quad (62)$$

where $p_\perp \equiv \sqrt{p_x^2 + p_y^2}$ is the transverse momentum. We ensure non-negativity of the phase-space distribution via the Θ function

$$f(\eta=0,\mathbf{p},\tau=\tau_0) = \frac{F(\xi)}{A_T\tau_0}\frac{dN}{d\eta}\frac{e^{-p/T}}{8\pi T^3}[1+\phi_G(\eta,\mathbf{p})] \times \Theta(1+\phi_G(\eta,\mathbf{p})), \quad (63)$$

where A_T is the transverse area of the system (with the elimination of negative phase-space contributions, a normalization factor $F(\xi) \leqslant 1$ is needed to set a given $dN/d\eta$). The cutoff does not affect the general scalings of transport solutions but does influence the initial pressure anisotropy [for example, values $R_p = 0.3$ and 1.75 set based on Eq. (62) change to $R_p \approx 0.476$ and 1.693 when the cutoff is applied]. Therefore, we initialize hydrodynamics with a shear stress π_L that gives the same initial pressure anisotropy as the transport.

The transport solutions were obtained using the MPC algorithm [39], which employs the particle subdivision technique to maintain covariance [26,28]. Transverse translational invariance was maintained in the calculation through periodic boundary conditions in the two transverse directions. A longitudinally boost-invariant system was initialized in a coordinate rapidity interval $-5 < \eta < 5$, and observables were calculated by averaging over $-2 < \eta < 2$ with proper Lorentz boosts of local quantities to $\eta = 0$.

A. Pressure anisotropy

Figure 1 shows the pressure anisotropy p_L/p_T evolution as a function of the rescaled proper time $\tilde{\tau} = \tau/\tau_0$ from the transport and Israel-Stewart hydrodynamics with the local equilibrium initial condition. The left panel shows calculations

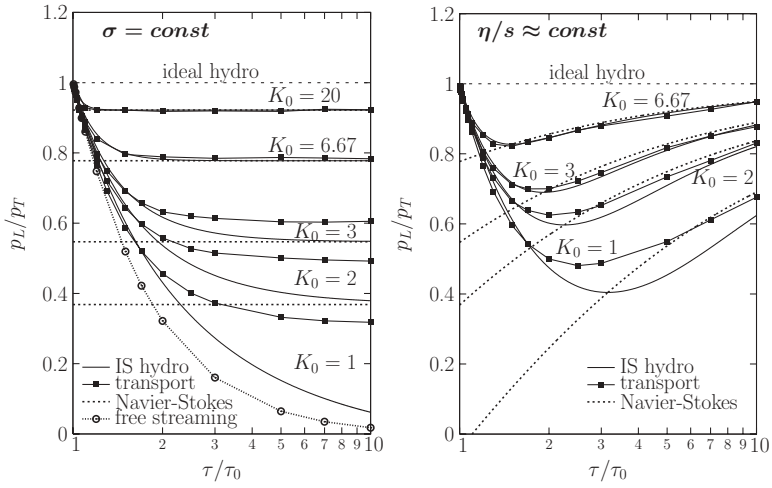

FIG. 1. Time evolution of pressure anisotropy $R_p \equiv p_L/p_T$ from covariant transport and Israel-Stewart dissipative hydrodynamics as a function of $K \equiv \tau/\lambda_{\rm tr}(\tau)$, from local equilibrium initial conditions $\pi_L(\tau_0) = 0$. Results for Navier-Stokes and free streaming are also shown. Left: $\sigma = {\rm const}$ scenario, for which the curves are labeled by $K(\tau) = {\rm const} = K_0 = 1, 2, 3, 6.67$, and 20. For $K = 1$, the Navier-Stokes result is negative and therefore not visible. Right: $\sigma \propto \tau^{2/3}$ scenario, for which $\eta_s/s_{\rm eq} \approx {\rm const}$ and the curves are labeled by the initial $K_0 = K(\tau_0) = 1, 2, 3$, and 6.67.

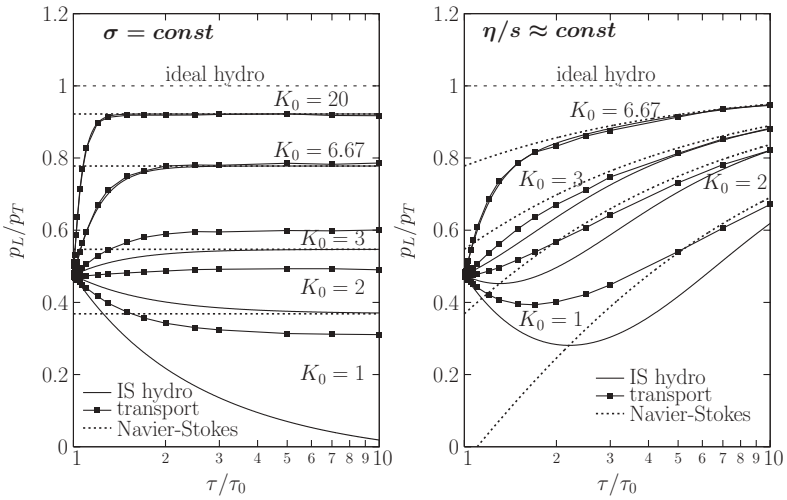

FIG. 2. Same as Fig. 1, but for an initial pressure anisotropy $R_p(\tau_0) = 0.476$ ($\xi_0 = -0.423$). In the $\sigma =$ const scenario, the NS curve for $K_0 = 1$ is negative and therefore not visible.

for the $\sigma =$ const scenario. For $K_0 = 1$, the anisotropy from IS hydro starts to fall rapidly below the transport above $\tau \gtrsim 2\tau_0$, and it is a factor of $\sim$5 smaller by late $\tau \sim 10\tau_0$. Clearly, the system cannot stay near equilibrium when the rate of scatterings equals the expansion rate. With increasing K_0, the undershoot becomes smaller and gradually vanishes as $K_0 \to \infty$. The difference is only $\sim$10% already at $K_0 = 3$ and is rather small by $K_0 \approx 7$.

The right panel shows the same but for the growing cross section scenario with $\eta_s/s_{\rm eq} \approx$ const. The situation of course improves because in this case K increases with time. For $K_0 = 1$, IS hydro undershoots the pressure anisotropy from the transport only by $\sim$20%, and the differences vanish at late times (since in this case both theories converge to $R_p = 1$ as $\tau \to \infty$). About 10% accuracy is achieved already for $K_0 = 2$, while for $K_0 = 3$, IS hydro is accurate to a few percent.

Moreover, the above findings hold for a wide range of initial conditions, including large initial pressure anisotropies, as shown in Figs. 2 and 3. These figures are for the same calculation but with $R_p(\tau_0) = 0.476$ and 1.693, respectively (which correspond to $\xi_0 = -0.423$ and 0.375). We emphasize that the results hold only if nonequilibrium corrections are close to the form (11) suggested by Grad. For such a class of initial conditions, however, we find that IS hydrodynamics can well approximate the transport ($\sim$10% accuracy) provided $K_0 \gtrsim 3$, even for the most pessimistic constant cross section scenario. If $\eta_s/s_{\rm eq} =$ const, only $K_0 \gtrsim 2$ is needed. We stress that in either case, there is no need for the initial conditions to be near the NS limit.

This is quite remarkable, because from Figs. 1–3 it is clear that already the early evolution differs between IS hydrodynamics and transport. For example, for an equilibrium initial condition ($\xi(\tau_0) = 0$), IS hydrodynamics of Eq. (44) gives

$$R_p^{\rm IS}(\tau) = 1 - \frac{4(\tau - \tau_0)}{3\tau_0} + \mathcal{O}((\tau - \tau_0)^2) \qquad (64)$$

for any initial value and evolution scenario for κ. From covariant transport, on the other hand (see Appendix D2),

$$R_p^{\rm transp}(\tau) = 1 - \frac{8(\tau - \tau_0)}{5\tau_0} + \mathcal{O}((\tau - \tau_0)^2). \qquad (65)$$

That is, pressure anisotropy develops, universally, 20% faster from the transport than from IS hydrodynamics (if the evolution starts from equilibrium).

This illustrates a limitation of the hydrodynamic description of transport solutions. Similar discrepancies were observed in Ref. [8] in the early evolution of differential elliptic flow

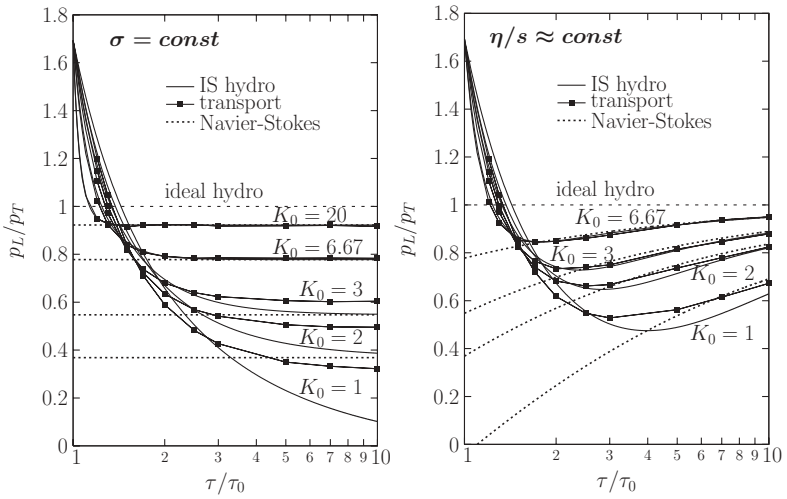

FIG. 3. Same as Fig. 1, but for an initial pressure anisotropy $R_p(\tau_0) = 1.693$ ($\xi_0 = 0.375$). In the $\sigma =$ const scenario, the Navier-Stokes curve for $K_0 = 1$ is negative and therefore not visible.

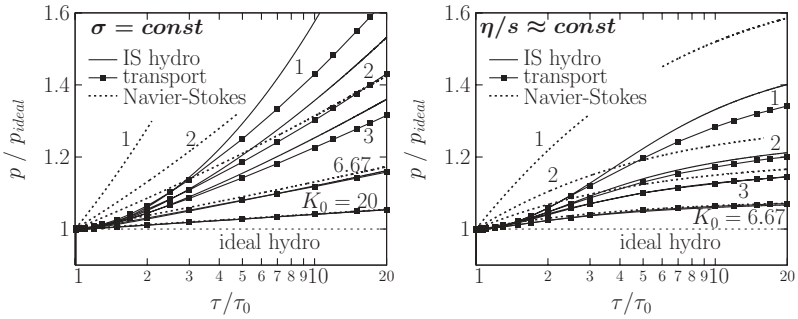

FIG. 4. Same as Fig. 1, except for the time evolution of the (average) pressure. The pressure is plotted normalized to the pressure $p_{\rm ideal}(\tau) = p_0(\tau_0/\tau)^{4/3}$ in ideal hydrodynamics.

$v_2(p_T)$. Remarkably, in our case, though the transport develops deviations from equilibrium faster, its rate of departure slows down quicker, which at intermediate times results in *smaller* accumulated dissipative corrections to the pressure anisotropy than from IS hydrodynamics. Eventually, the hydrodynamic evolution "catches up" to the transport, except for low $K \lesssim 3$ in the $\sigma =$ const scenario.

Figures 1–3 also show the Navier-Stokes approximation for each of the Israel-Stewart results. By late times, the NS and IS solutions converge for both cross section scenarios, independently of the initial pressure anisotropy (for $\sigma =$ const and $K_0 = 1$, the NS anisotropy is negative and therefore not visible in the plots). However, the applicability of NS theory at early times depends, besides on the value of K_0, strongly on how far the initial shear stress is from its NS value [Eq. (39)]. Navier-Stokes assumes that shear stress and, therefore, the pressure anisotropy relax immediately, but relaxation happens over a finite time. The approach toward the Navier-Stokes limit is governed by $\tau_\pi = 3\tau/(2\kappa)$, therefore *Navier-Stokes becomes applicable only after some time* $\Delta\tau \sim |R_0 - R_{\rm NS}|\tau_0/\kappa$. Note that the initial slope of the $R(\tau)$ curves does not always reflect τ_π directly, because it is given by the initial derivative of ξ

$$\dot{R}(\tau) \sim \frac{3}{2}\dot{\xi}(\tau) = -\frac{3}{2\tau_\pi}(\xi - \xi_{\rm NS}) + \mathcal{O}(1)\frac{\xi}{\tau}, \qquad (66)$$

where we combined Eqs. (26) and (35), incorporated the observations that $Y_\pi \sim \mathcal{O}(1)/\tau$ and $Z_\pi = 0$, and assumed ξ is small. For local equilibrium initial conditions, the slope of $R(\tau)$ is therefore $\sim\mathcal{O}(1)\xi_{\rm NS}/\tau_\pi \sim \mathcal{O}(1)/\tau$, independently of K_0 [cf. Fig. 1 and Eq. (64)]. For initial shear stresses far from the NS limit, on the other hand, the slope $\sim\mathcal{O}(1)\xi/\tau_\pi \propto \kappa$ steepens with increasing K as seen in Figs. 2 and 3.

The inaccurate description of early shear stress evolution in Navier-Stokes has a cumulative effect on the evolution of thermodynamic quantities, such as the pressure and the entropy, as we show in the next two sections. Of course, the errors are proportional to the ratio of the time the system spends away from the NS limit and the hydrodynamic time scale, i.e., $\Delta\tau/\tau_0 \sim 1/\kappa$.

B. Pressure evolution

Now we turn to the evolution of the (average) pressure. In ideal hydrodynamics ($K_0 \to \infty$), the pressure drops rapidly with time $p_{\rm id} \propto \tau^{-4/3}$. Therefore it is more convenient to study dissipative effects *relative* to ideal hydrodynamics through the ratio $p(\tau)/p_{\rm id}(\tau)$.

Figure 4 shows the pressure relative to that in ideal hydrodynamics as a function of the rescaled proper time $\tilde{\tau} = \tau/\tau_0$ from the transport and IS hydrodynamics with the local equilibrium initial condition. For the $\sigma =$ const scenario, for all K_0 values, the evolution starts out the same between IS hydrodynamics and transport but then the IS starts to accumulate deviations, because it follows the shear stress evolution only approximately. For $K_0 = 1$, IS hydrodynamics maintains 10% accuracy in the magnitude of dissipative *corrections* (i.e., $p/p_{\rm id} - 1$) only up to $\tau \approx 4\tau_0$. As K_0 increases, the situation improves gradually: for $K_0 = 3$, 10% accuracy holds up to $\tau \approx 10\tau_0$, and by $K_0 \approx 7$ the IS stays within a few percent of the transport even until $\tau = 20\tau_0$.

For the growing cross section scenario with $\eta_s/s_{\rm eq} \approx$ const, we see in Fig. 4 that hydrodynamic has a wider range of applicability. This is because $K \sim \tau^{2/3}$ grows with time. For $K_0 = 1$, the error in the dissipative correction $(p/p_{\rm id} - 1)$ is less than 10% up to $\tau \approx 5\tau_0$, and already for $K_0 = 2$, IS hydrodynamics is accurate to within better than 10% throughout the whole range $\tau \leqslant 20\tau_0$ studied. The pressure evolution results therefore reinforce the regions of validity found in the previous section ($K_0 \gtrsim 3$ for $\sigma =$ const, and $K_0 \gtrsim 2$ for $\eta_s/s_{\rm eq} \approx$ const).

Clearly, the region of applicability for Navier-Stokes is more limited (Fig. 4). For low K_0, it overestimates the pressure corrections not only at late times but also at early $\tau \sim$ few $\times\ \tau_0$. $K_0 \approx 7$ is barely sufficient for 10% accuracy in viscous corrections for $\eta_s/s_{\rm eq} \approx$ const, but it is not enough in the case of $\sigma =$ const. Based on the trends with increasing K_0, we estimate that $K_0 \gtrsim$ 9–10 is needed for Navier-Stokes with $\sigma =$ const to deviate less than 10% from the viscous effects calculated with the transport. Therefore, for local equilibrium initial conditions, Navier-Stokes theory becomes applicable at about three times shorter mean free paths, or equivalently three times larger longitudinal proper time τ (i.e., three times slower longitudinal expansion), than Israel-Stewart theory.

C. Entropy

Now we proceed with results on entropy production. In transport theory, the entropy current is defined as

$$S^\mu(x) = -\int \frac{d^3p}{p^0} p^\mu f(x,\mathbf{p}) \left[\ln\left(\frac{(2\pi)^3}{g} f(x,\mathbf{p})\right) - 1\right], \qquad (67)$$

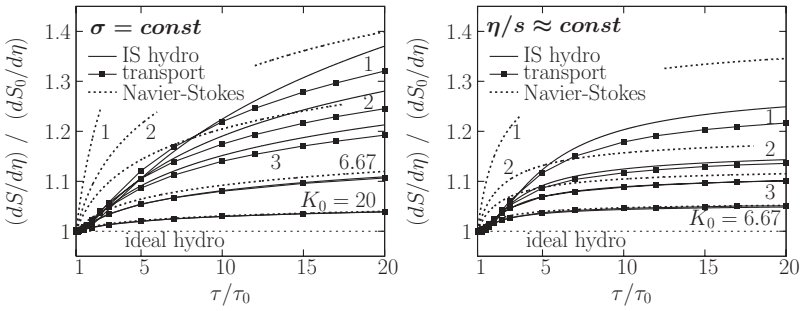

FIG. 5. Same as Fig. 1 except for the time evolution of the entropy per unit rapidity, normalized by its initial value (note the linear time axis used this time). For the transport solutions, entropy was calculated approximately using the IS entropy expression (50). Chemically equilibrated initial conditions (i.e., $\chi_0 = 0$) were assumed.

where g is the number of internal degrees of freedom. This nonlinear function of the phase-space density f is cumbersome to evaluate with the MPC code, and therefore we here opt for an approximate result based on the truncated IS expression (50), evaluated using the pressure and shear stress from the transport. This includes dissipative corrections to the entropy up to quadratic order in ϕ.

In the most dissipative $\sigma = \text{const}$ scenario with $K_0 = 1$, there is about 30% additional entropy produced by late times $\tau/\tau_0 \sim 10$–20, as can be seen in Fig. 5. For $\eta_s/s_{\text{eq}} \approx \text{const}$, the same $K_0 = 1$ yields only about 20% extra entropy. With increasing K_0, entropy generation gradually weakens, and by $K_0 \sim 7$ it is only 10% and 5%, respectively.

The Israel-Stewart results are within 15% of the approximate transport results already for $K_0 = 1$, and about 10% accuracy in the calculated dissipative effect is achieved for $K_0 \gtrsim 3$ (for $\sigma = \text{const}$) and $K_0 \gtrsim 2$ (for $\eta_s/s_{\text{eq}} \approx \text{const}$). In contrast, the Navier-Stokes strongly overpredicts the entropy, unless K_0 exceeds about 6 for $\sigma = \text{const}$ or ≈ 3 for $\eta_s/s_{\text{eq}} \approx \text{const}$. The bounds for 10% accuracy are in agreement with those found previously in Sec. V B.

D. Limitations of the naive Israel-Stewart approximation

Now we discuss the applicability of the "naive" Israel-Stewart equations. Figure 6 compares the pressure evolution in complete Israel-Stewart theory to that in the naive approximation, for local equilibrium initial conditions ($\xi_0 = 0$), as a function of the rescaled proper time τ/τ_0. Clearly, the naive result overshoots the pressure both for the constant cross section scenario and for $\eta_s/s_{\text{eq}} \approx \text{const}$, unless K_0 is large. This confirms expectations based on the analytic solutions in Appendix C. Though the naive theory converges to the correct result at large enough $K_0 \sim 7$–20, comparison with Fig. 4 tells us that it is even less accurate than Navier-Stokes theory.

Similar behavior has also been observed in a 2 + 1D calculation [35] that found that the naive approximation leads to larger dissipative effects on the *transverse* momentum anisotropy than the complete Israel-Stewart theory.

The reason for the large errors is that away from local equilibrium the naive approach drives the shear stress more negative [compare Eqs. (36) and (41), and note that typically $\pi_L < 0$]. For the 0 + 1D expansion studied here ($Y_\pi < 0$ and $Z_\pi = 0$), at early times, complete IS theory drives shear stress toward a value that is less negative than shear stress in Navier-Stokes; whereas at late times, the complete theory can keep the system closer to local equilibrium, because its effective shear stress relaxation time is shorter [see discussion in Ref. [12], or cf. Eq. (26)]. This is demonstrated in Fig. 7 where we plot the pressure anisotropy R_p, which is a monotonic function of $\xi = \pi_L/p$. For $\sigma = \text{const}$, we find that the naive approach saturates the anisotropy at a lower value than the complete theory, confirming the analytic expectations in Appendix C1. For $\eta_s/s_{\text{eq}} \approx \text{const}$, the system does approach ideal hydrodynamic behavior eventually; however, that occurs on a much longer time scale than from complete IS theory. This is in agreement with the expectation based on the analytic solutions (C35)–(C38).

The pressure anisotropy results further reinforce our conclusion that the naive Israel-Stewart approximation is poorer than Navier-Stokes (cf. Fig. 1). In heavy ion collisions, gradients are large, at least initially, and therefore cannot be ignored even if dissipative corrections (e.g., π_L/p) are small.

E. Implications for heavy ion physics

Having determined the region of validity (defined as 10% accuracy in dissipative effects) for IS and NS hydrodynamics in terms of the initial ratio of the expansion and scattering time scales $K_0 = \tau_0/\lambda_{\text{tr},0}$

$$K_0^{\text{IS}} \gtrsim 3, \quad K_0^{\text{NS}} \gtrsim 9 \quad (\sigma = \text{const}), \tag{68}$$

$$K_0^{\text{IS}} \gtrsim 2, \quad K_0^{\text{NS}} \gtrsim 6 \quad (\eta_s/s_{\text{eq}} \approx \text{const}), \tag{69}$$

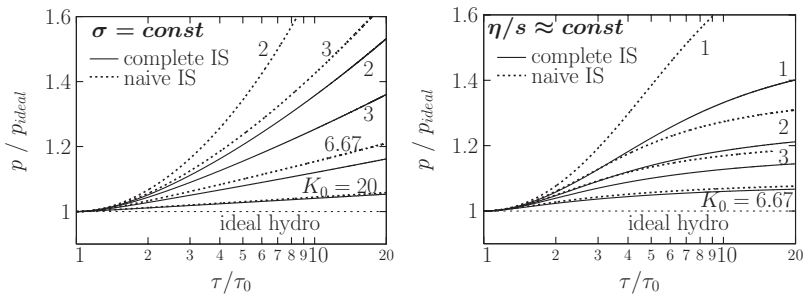

FIG. 6. Time evolution of the (average) pressure from complete IS theory and the naive IS approximation as a function of $K \equiv \tau/\lambda_{\text{tr}}(\tau)$, for local equilibrium initial conditions $\pi_L(\tau_0) = 0$. The pressure is plotted normalized to the pressure $p_{\text{id}}(\tau) = p_0(\tau_0/\tau)^{4/3}$ in ideal hydrodynamics. In the $\sigma = \text{const}$ scenario, $K(\tau) = \text{const} = K_0 = 2, 3, 6.67$, and 20. In the $\sigma \propto \tau^{2/3}$ scenario, $\eta_s/s_{\text{eq}} \approx \text{const}$ and the curves are labeled by the initial $K_0 = K(\tau_0) = 1, 2, 3$, and 6.67.

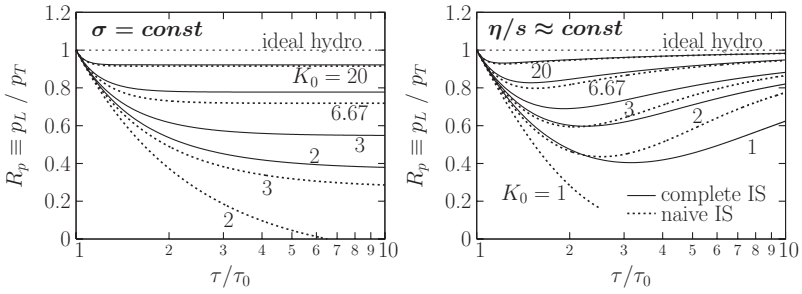

FIG. 7. Same as Fig. 6, but for the time evolution of the pressure anisotropy.

we now turn to implications for heavy ion collisions. From Eqs. (37), (51), and (52),

$$\kappa_0 = \frac{T_0\tau_0}{4-\chi_0}\frac{s_0}{\eta_{s,0}} \approx 15.9 \times \frac{1}{1-\chi_0/4}\left(\frac{T_0}{1\ \text{GeV}}\right)\left(\frac{\tau_0}{1\ \text{fm}}\right)\left(\frac{1/(4\pi)}{\eta_{s_0}/s_0}\right), \quad K_0 \approx 0.8\kappa_0. \tag{70}$$

Therefore, we can place an upper limit on the (initial) shear viscosity for which IS or NS reproduces with better than 10% accuracy the viscous corrections to basic observables such as pressure and entropy: for $\sigma = \text{const}$,

$$\left.\frac{4\pi\eta_{s,0}}{s_{\text{eq},0}}\right|_{\text{IS}} \lesssim 0.8T_0\tau_0, \qquad \left.\frac{4\pi\eta_{s,0}}{s_{\text{eq},0}}\right|_{\text{NS}} \lesssim 0.25T_0\tau_0, \tag{71}$$

while for $\eta_s/s_{\text{eq}} \approx \text{const}$,

$$\left.\frac{4\pi\eta_s}{s_{\text{eq}}}\right|_{\text{IS}} \lesssim 1.2T_0\tau_0, \qquad \left.\frac{4\pi\eta_s}{s_{\text{eq}}}\right|_{\text{NS}} \lesssim 0.4T_0\tau_0, \tag{72}$$

where we assumed chemical equilibrium initial conditions ($\chi_0 = 0$). If the shear viscosity of dense quark-gluon matter is bounded from below by $4\pi\eta_s/s_{\text{eq}} \gtrsim 1$, as has been conjectured recently, then the situation for Israel-Stewart theory is close to marginal. For $\eta_s/s_{\text{eq}} = 1/(4\pi)$, typical parton transport initial conditions ($T_0 = 0.7$ GeV, $\tau_0 = 0.1$ fm) translate into $K_0 \lesssim 1$, for which IS is not applicable for either scenario I or II; whereas for typical hydrodynamic initial conditions ($T_0 \sim 0.38$ GeV, $\tau_0 = 0.6$ fm), we have $K_0 \lesssim 3$, sufficient for both scenarios (barely for $\sigma = \text{const}$).

On the other hand, Navier-Stokes may be marginally applicable only if $\eta_s/s_{\text{eq}} \lesssim 0.5/(4\pi)$ throughout the whole evolution, at least based on this 0 + 1D study, where acausal artifacts and instabilities do not arise. We emphasize that the bound quoted here is for initial conditions close to local equilibrium. The accuracy of the NS approximation strongly depends on how far the initial shear stress is from the NS value. If the evolution starts out near the NS limit, we expect Navier-Stokes to be accurate up to higher viscosities.

Within the region of applicability of the Israel-Stewart theory, dissipative corrections to the average pressure and the entropy are modest and stay below ∼20% even up to late times $\tau \leqslant 10\tau_0$. This may serve as a useful "rule of thumb" applicability condition for hydrodynamics: if dissipative corrections to average pressure and the entropy calculated from hydrodynamics are significantly larger than 20%, the validity of hydrodynamics is questionable.

The above findings reinforce a recent calculation [18] in 2 + 1D that found good agreement between IS hydrodynamics and 2 → 2 transport, for conditions expected in Au + Au at $\sqrt{s_{NN}} \sim 200$ GeV/nucleon at RHIC, in the case of a small shear viscosity to entropy density ratio $\eta_s/s_{\text{eq}} \approx 1/(4\pi)$ (on average). The same study also found good agreement between the two theories for a large constant transport cross section $\sigma_{\text{tr}} \approx 13$ mb. That is also in line with our results here, because it corresponds to $4\pi\eta_s/s_{\text{eq}}(\tau_0) \approx 0.25$ in the center of the collision zone, i.e., initially $\eta_s/s_{\text{eq}} \lesssim 1/(4\pi)$ in most of the system.

Finally we note that the applicability of the hydrodynamic approach on very short time and length scales is another important question. In typical real-life problems, $T_0\tau_0 \gg 1$ because the hydrodynamic expansion time scale τ is by orders of magnitude larger than the quantum (energy) time scale $1/T$. This also leaves ample room to make hydrodynamics applicable ($\kappa_0 \gg 1$) even for appreciable viscosities. In the heavy ion case, however, the two time scales are comparable $T_0\tau_0 \sim \mathcal{O}(1)$, and therefore a macroscopic treatment may be marginal.

VI. CONCLUSIONS

Based on comparison to covariant transport theory, we explore the region of validity of Israel-Stewart and Navier-Stokes hydrodynamics in heavy-ion physics applications. We follow the evolution of the average pressure, pressure anisotropy, and entropy for a massless ideal gas in 0 + 1D longitudinally expanding Bjorken geometry. Binary 2 → 2 interactions are considered for two main scenarios, a fixed cross section $\sigma = \text{const}$ (scenario I, pessimistic for hydrodynamics) and a scale-invariant system with $\eta_s/s_{\text{eq}} \approx \text{const}$ (scenario II, optimistic for hydrodynamics).

We find (Sec. V) that dissipative effects calculated from IS hydrodynamics reproduce those from the transport solutions to within 10%, provided initially the expansion time scale is three (for scenario I) or two (for scenario II) times larger than the transport mean free path, i.e., the initial inverse Knudsen number $K_0 = \tau_0/\lambda_{\text{tr},0} \gtrsim 3$ or 2. When this criterion is fulfilled, Israel-Stewart is accurate even if initial pressure anisotropies are large $p_L/p_T \sim 0.4$–1.7, there is no need to start near the Navier-Stokes limit. On the other hand, the same accuracy from Navier-Stokes requires three times larger K_0, if the expansion starts from the local thermal equilibrium (unlike for Israel-Stewart, the applicability of Navier-Stokes depends strongly on how far the initial shear stress is from its NS

value). We emphasize that these findings apply only when *initial* viscous corrections are of the quadratic form suggested by Grad [Eq. (11)].

These results imply that (Sec. V E) for typical heavy ion initial conditions at RHIC energies, Israel-Stewart hydrodynamics is accurate up to $\eta_s/s_{\rm eq} \lesssim 1.5/(4\pi)$, while for Navier-Stokes, $\eta_s/s_{\rm eq} \lesssim 0.5/(4\pi)$ is needed. This is supported by a recent 2 + 1D calculation [18] that finds good agreement between IS and transport for $\eta_s/s_{\rm eq} \approx 1/(4\pi)$, and also for a large $\sigma_{\rm tr} \approx 13$ mb.

In addition, we test the accuracy of the naive IS approximation (Sec. V D) that neglects products of gradients and dissipative quantities in the equations of motion and find that it has an even more limited applicability than Navier-Stokes.

We also compare in detail (Appendix C) the IS and NS solutions in 0 + 1D for four scenarios, $\sigma = \text{const}$, $\sigma \propto 1/T^2$, $\sigma \propto \tau^{2/3}$, and $\eta_s/s_{\rm eq} = \text{const}$, and find that results for the latter two are almost identical, even at low initial Knudsen numbers $\sim$1. Moreover, we obtain analytic IS and NS solutions in 0 + 1D, which are useful for quick estimates (Secs. IV B and IV C) and to test numerical solution techniques. We also derive additional tests (Appendix B) based on generalized conservation laws for conserved currents, energy-momentum, and entropy, which can be utilized to verify the accuracy of numerical IS solvers in 1 + 1, 2 + 1, and 3 + 1 dimensions.

Finally we emphasize that the current study is limited to a massless ideal gas with particle number conserving interactions in 0 + 1D Bjorken geometry. The influence of the transverse expansion will be quantified in a future paper (requires at minimum a 1 + 1D approach). It will also be important to check how the results depend on the equation of state and the presence of particle nonconserving processes, such as radiative $2 \leftrightarrow 3$. For a nonconformal equation of state, bulk viscosity may become important [40,41]. Ideally, one should also test the accuracy of the hydrodynamic approximation for nonequilibrium theories other than covariant transport.

ACKNOWLEDGMENTS

We thank RIKEN, Brookhaven National Laboratory, and the US Department of Energy [DE-AC02-98CH10886] for providing facilities essential for the completion of this work. We also thank the hospitality of INT/Seattle (D.M., P.H.), KFMI/RMKI (D.M.), and Iowa State University (P.H.) where parts of this work were completed. Computational resources managed by RCAC/Purdue are also gratefully acknowledged.

APPENDIX A: ORIGIN OF a_0, a_1, a_0', a_1' IN THE IS EQUATIONS OF MOTION

The equations of motion (23)–(25) reproduce the entropy production rate of Eq. (16) only approximately, up to typically small quartic and higher-order corrections in dissipative quantities. With $a_i \equiv 0 \equiv a_i'$, a contribution

$$\Pi q^\mu T\nabla_\mu(\alpha_0/T) - q_\nu \pi^{\nu\mu} T\nabla_\mu(\alpha_1/T) \tag{A1}$$

would be *missing* from $T\partial_\mu S^\mu$ in Eq. (16). These terms are bilinear in the dissipative quantities and, therefore, can be split arbitrarily between the bulk pressure and heat, and heat and shear equations of motion. That is, with

$$T\nabla^\mu(\alpha_i/T) \equiv a_i^\mu + a_i'^\mu \tag{A2}$$

Eq. (16) is identically satisfied but contributions to the equations of motion depend on a_i

$$\beta_0 D\Pi = (\cdots) + a_0'^\mu q_\mu, \tag{A3}$$

$$\beta_1 Dq^\mu = (\cdots) + \Delta^\mu_\nu a_0{}^\nu \Pi - a_1^\nu \pi^\mu_\nu, \tag{A4}$$

$$\beta_2 D\pi^{\mu\nu} = (\cdots) - a_1'^{\langle\nu} q^{\mu\rangle}. \tag{A5}$$

Only components orthogonal to u^μ contribute, but apart from that constraint, a_0^μ and a_1^μ are arbitrary functions of the hydrodynamic fields and their derivatives and potentially new scalar functions $\{a_i^{(k)}(\varepsilon, n)\}$ characterizing an isotropic matter. However, ignoring the dependence on the dissipative quantities is consistent with the truncation of the entropy current [Eq. (14)] at quadratic order in those. Moreover, for small deviations from equilibrium, one may seek to include only the leading contributions coming from first derivatives of the ideal hydrodynamic fields, i.e.,

$$a_i^\nu = a_i^{(1)} Du^\nu + a_i^{(2)} T\nabla^\nu \frac{1}{T} + a_i^{(3)} \nabla^\nu \frac{\mu}{T}, \tag{A6}$$

where we chose $1/T$ and μ/T as the two independent variables instead of ε and n. But the three terms are not independent: energy-momentum conservation [Eq. (1)] and the Gibbs-Duhem relation $s\,dT = dP - n\,d\mu$ provide one constraint

$$\frac{1}{T}\Delta^{\nu\alpha} Du_\alpha + \nabla^\nu \frac{1}{T} = \frac{n}{\varepsilon + p}\nabla^\nu \frac{\mu}{T}, \tag{A7}$$

and $\nabla^\nu(\mu/T)$ may be ignored, at least parametrically, because it is proportional to the heat flow [Eq. (4)] in the first-order (Navier-Stokes) theory. Therefore, to leading accuracy only one scalar function enters, and we can write

$$a_i^\mu = -a_i(\varepsilon, n) Du^\mu. \tag{A8}$$

Analogous arguments give

$$T\nabla^\nu(\alpha_i/T) \approx T\frac{\partial(\alpha_i/T)}{\partial(1/T)}\nabla^\nu \frac{1}{T} \approx -\frac{\partial(\alpha_i/T)}{\partial(1/T)}\nabla^{\nu\alpha} Du_\alpha, \tag{A9}$$

from which Eq. (20) follows.

We plan to revisit the above approximations in a future study. In any case, they do not influence our 0 + 1D calculations here, because the a_i terms do not play a role (heat flow vanishes by symmetry).

APPENDIX B: GENERALIZED CONSERVATION LAWS

Here we present general relations of the form

$$\frac{d\mathcal{A}(\tau)}{d\tau} = \mathcal{B}(\tau), \tag{B1}$$

which can be used to test the accuracy of numerical dissipative hydrodynamics solutions in any dimensions. $\mathcal{A}$ and $\mathcal{B}$ only

depend on the hydrodynamic fields at the given τ. Evaluating them at each time step, one can either numerically differentiate $\mathcal{A}(\tau)$ or integrate $\mathcal{B}(\tau)$ and check how accurately the solutions satisfy Eq. (B1).

Consider a four-divergence $\partial_\mu A^\mu(x)$ (in regular Minkowski coordinates). Integration over a four-volume V_4 gives

$$\int_{V_4} d^4x \partial_\mu A^\mu(x) = \int_{\sigma(V_4)} d\sigma_\mu(x) A^\mu(x), \tag{B2}$$

where $\sigma(V_4)$ is the three-dimensional boundary ("surface") of V_4. Now take the special case of a Bjorken "box" $V_4 = \Delta\tau \times \Delta\eta \times A_T$ with an infinite transverse area $A_T \to \infty$ but infinitesimal proper time and finite coordinate rapidity extensions $\Delta\tau \to 0$, $\Delta\eta = \eta_2 - \eta_1$. Assuming $A^\mu(x)$ drops faster than $1/x_T^2$ at large $|\mathbf{x}_T|$, we can neglect surface terms at $|\mathbf{x}_T| \to \infty$ and keep only contributions on $\tau = \text{const}$ and $\eta = \text{const}$ hypersurfaces:

$$\begin{aligned}\int d\tau\, \tau d\eta\, dx_T^2\, \partial_\mu A^\mu(x) &= \left[\int_{\sigma(\tau+d\tau)} d\sigma_\mu^{(\tau)} - \int_{\sigma(\tau)} d\sigma_\mu^{(\tau)}\right. \\ &\quad \left. + \int_{\sigma(\eta_2)} d\sigma_\mu^{(\eta)} - \int_{\sigma(\eta_1)} d\sigma_\mu^{(\eta)}\right] A^\mu(x)\end{aligned} \tag{B3}$$

where the surface normals are

$$\begin{aligned} d\sigma^\mu_{(\tau)} &= \tau\, dx_T^2\, d\eta u_B^\mu, \quad d\sigma^\mu_{(\eta)} = -d\tau\, dx_T^2\, u_3^\mu, \\ \text{with} \quad u_B^\mu &\equiv (\text{ch}\,\eta, \mathbf{0}, \text{sh}\,\eta), \quad u_3^\mu \equiv (\text{sh}\,\eta, \mathbf{0}, \text{ch}\,\eta), \end{aligned} \tag{B4}$$

and we used $d^4x = d\tau\, \tau\, d\eta\, dx_T^2$. Here, u_B is the longitudinal Bjorken flow velocity, while u_3 is its orthonormal counterpart in the t-z plane. Note that the actual flow velocity does *not* need to be u_B. Dividing by $\Delta\tau$ and taking the limit, we arrive at

$$\begin{aligned}\tau \int d\eta\, dx_T^2\, \partial_\mu A^\mu &= \partial_\tau \left(\tau \int d\eta\, dx_T^2\, u_B^\mu A_\mu\right) \\ &\quad - \int dx_T^2\, u_3^\mu (A_\mu(\eta_1) - A_\mu(\eta_2)),\end{aligned} \tag{B5}$$

which is a generalized conservation law for the quantity

$$\mathcal{A} \equiv \tau \int d\eta dx_T^2\, u_B^\mu A_\mu. \tag{B6}$$

If $\partial_\mu A^\mu \equiv 0$, and the surface term $u_3^\mu(A_\mu(\eta_1) - A_\mu(\eta_2))$ vanishes, we have $\mathcal{A}(\tau) = \text{const}$.

In a boost-invariant calculation, the longitudinal extension of the system is formally infinite, and thus a generalized conservation law for a quantity per unit rapidity is more practical. It can be obtained in a similar fashion if one divides by $\Delta\eta$ and takes the limit $\Delta\eta \to 0$. The result is

$$\tau \int dx_T^2\, \partial_\mu A^\mu = \partial_\tau \frac{d\mathcal{A}}{d\eta} - \partial_\eta \int dx_T^2\, u_3^\mu A_\mu, \tag{B7}$$

where

$$\frac{d\mathcal{A}}{d\eta} = \tau \int dx_T^2\, u_B^\mu A_\mu. \tag{B8}$$

Again, if $\partial_\mu A^\mu \equiv 0$ and the η-derivative term vanishes, we have $d\mathcal{A}/d\eta = \text{const}$.

1. Charge/particle number

We first apply Eq. (B5) to a *conserved* current in the Eckart frame: $N^\mu = n_{\text{eq}} u^\mu$, where $u^\mu = \gamma(\text{ch}\,\theta, v\mathbf{e}_R, \text{sh}\,\theta)$ is the flow four-velocity and θ is the flow rapidity. Now $u_B^\mu u_\mu = \gamma\, \text{ch}(\eta - \theta)$ and $u_3^\mu u_\mu = \gamma\, \text{sh}(\eta - \theta)$. If the rapidity interval is so large that $N^\mu(\eta_1) = N^\mu(\eta_2) = 0$, or the system is boost invariant, $\eta \equiv \theta$, the surface terms are zero, and we get a simple conservation law

$$N = \tau \int d\eta\, dx_T^2\, \gamma n\, \text{ch}(\eta - \theta) = \text{const}. \tag{B9}$$

In a boost-invariant case, the coordinate rapidity integral is trivial, and we obtain

$$\frac{dN}{d\eta} = \tau \int dx_T^2 \gamma n = \text{const}. \tag{B10}$$

2. Entropy

Second, we apply Eq. (B5) to the entropy current of Eq. (14) and its divergence in Eq. (16). If $S^\mu(\eta_1) = S^\mu(\eta_2) = 0$, we get

$$\partial_\tau S = \tau \int d\eta\, dx_T^2 \left(\frac{\Pi^2}{\zeta T} - \frac{q_\mu q^\mu}{\kappa_q T^2} + \frac{\pi_{\mu\nu}\pi^{\mu\nu}}{2\eta_s T}\right) \geqslant 0, \tag{B11}$$

where the entropy of the system is

$$S = \tau \int d\eta\, dx_T^2\, u_B^\mu S_\mu, \tag{B12}$$

and the last inequality follows from the general properties $q^\mu q_\mu \leqslant 0$ and $\pi^{\mu\nu}\pi_{\mu\nu} \geqslant 0$.

For longitudinally boost-invariant dynamics, it is more natural to follow entropy per unit rapidity:

$$\begin{aligned}\frac{dS}{d\eta} &= \tau \int dx_T^2 u_B^\mu S_\mu, \\ \partial_\tau \left(\frac{dS}{d\eta}\right) &= \tau \int dx_T^2 \left(\frac{\Pi^2}{\zeta T} - \frac{q_\mu q^\mu}{\kappa_q T^2} + \frac{\pi_{\mu\nu}\pi^{\mu\nu}}{2\eta_s T}\right) \geqslant 0.\end{aligned} \tag{B13}$$

3. Energy-momentum

Finally we derive the conservation equation corresponding to energy-momentum conservation $\partial_\mu T^{\mu\nu} = 0$. Contraction of the energy-momentum tensor with u_B^μ gives the conservation of energy. When the entire system is within the interval $[\eta_1, \eta_2]$, then

$$\partial_\tau E \equiv \partial_\tau \left(\tau \int d\eta\, dx_T^2\, u_B^\mu T_{\mu\nu}\, u_B^\nu\right) = 0. \tag{B14}$$

Contraction with $u_R^\mu \equiv (0, \mathbf{e}_R, 0)$ gives the change in transverse radial momentum. Substituting

$$\partial_\mu (T^{\mu\nu} u_{R,\nu}) = 0 + T^{\mu\nu} \partial_\mu u_{R,\nu} \tag{B15}$$

into Eq. (B5) results in

$$\begin{aligned}\partial_\tau M_r &\equiv \partial_\tau \left(\tau \int d\eta\, dx_T^2\, u_B^\mu T_{\mu\nu} u_R^\nu\right) \\ &= \tau \int d\eta\, dx_T^2 T^\mu{}_\nu \partial_\mu u_R^\nu.\end{aligned} \tag{B16}$$

To be more specific, we also show as an example a boost-invariant, cylindrically symmetric case. In the Landau frame,

$$T^{\mu\nu} = (\varepsilon + p + \Pi)u^\mu u^\nu - (p + \Pi)g^{\mu\nu} + (-\tilde{\pi}_2 - \tilde{\pi}_3)u_1^\mu u_1^\nu + \tilde{\pi}_2 u_2^\mu u_2^\nu + \tilde{\pi}_3 u_3^\mu u_3^\nu, \tag{B17}$$

where u_1 is the orthonormal counterpart of the flow velocity in the time-radial plane, while u_2 and u_3 are orthonormal counterparts of these in the axial and beam (rapidity) direction:

$$u^\mu = \gamma(\mathrm{ch}\,\eta, v\,\mathbf{e}_R, \mathrm{sh}\,\eta), \quad u_1^\mu = \gamma(v\,\mathrm{ch}\,\eta, \mathbf{e}_R, v\,\mathrm{sh}\,\eta),$$
$$u_2^\mu = (0, \mathbf{e}_\phi, 0), \quad u_3^\mu = (\mathrm{sh}\,\eta, \mathbf{0}, \mathrm{ch}\,\eta). \tag{B18}$$

These vectors are normalized to $u^2 = 1, u_1^2 = u_2^2 = u_3^2 = -1$. The viscous pressure tensor components in the fluid rest frame are $\pi^{\mu\nu}_{\mathrm{LR}} = \mathrm{diag}(0, -\tilde{\pi}_2 - \tilde{\pi}_3, \tilde{\pi}_2, \tilde{\pi}_3)$. It is important to notice that the surface terms in Eq. (B5) or the η-derivative term in Eq. (B7) are now nonzero. Contraction by u_B^μ as above and substitution into Eq. (B7) gives the evolution of the energy per unit rapidity:

$$\partial_\tau\left(\frac{dE}{d\eta}\right) \equiv \partial_\tau\left(\tau\int dx_T^2 T^{00}(\eta{=}0)\right) = -\int dx_T^2 (p + \Pi + \tilde{\pi}_3). \tag{B19}$$

Contraction by u_R^μ gives the evolution of transverse radial momentum per unit rapidity:

$$\partial_\tau\left(\frac{dM_r}{d\eta}\right) \equiv \partial_\tau\left(\tau\int dx_T^2 T^{01}(\eta{=}0, \phi{=}0)\right) = \tau\int dx_T^2 \frac{p + \Pi + \tilde{\pi}_2}{R}, \tag{B20}$$

where we have used the relations

$$u_B^\mu T_{\mu\nu} u_R^\nu = -T^{01}(\eta{=}0, \phi{=}0), \quad \partial_\mu u_R^\nu = -\frac{1}{R}u_{2,\mu}u_2^\nu. \tag{B21}$$

The above results reflect general expectations. Particle number per unit rapidity $dN/d\eta$ is strictly conserved in both the ideal and the dissipative case. Entropy per unit rapidity $dS/d\eta$ is conserved for an ideal fluid but increases if there is dissipation. In both cases, the energy per unit rapidity $dE/d\eta$ decreases because of longitudinal work, while the radial momentum per unit rapidity $dM_r/d\eta$ increases as a result of the buildup of radial flow, *as long as the system stays near equilibrium* (i.e., the total pressure is dominated by the ideal part).

APPENDIX C: VISCOUS SOLUTIONS FOR VARIOUS CROSS-SECTION SCENARIOS

Next we analyze viscous Israel-Stewart and Navier-Stokes solutions for four different types of cross section: constant, $\sigma \propto 1/T^2$, $\sigma \propto \tau^{2/3}$, and $\eta_s/s_{\mathrm{eq}} = \mathrm{const}$. For convenience, we will often use normalized quantities

$$\tilde{A}(\tau/\tau_0) \equiv \frac{A(\tau)}{A(\tau_0)}. \tag{C1}$$

We will show that for typical observables of interest (average pressure, pressure anisotropy, entropy, and shear viscosity to entropy ratio), $\eta_s/s_{\mathrm{eq}} = \mathrm{const}$ dynamics is well approximated by $\sigma \propto \tau^{2/3}$ already for $K_0 = 1$.

In analytic considerations, it will be often convenient to drop the π_L^2 term in the equations of motion (35) and (36), which is a good approximation for $|\pi_L| \ll p$, i.e., the general region of validity of viscous hydrodynamics. This should not be confused with the naive Israel-Stewart approximation, which also ignores the 4/3 factor in Eq. (36). For the $\sigma \propto \tau^{2/3}$ and $\sigma = \mathrm{const}$ scenarios, we obtain in this way accurate approximate analytic IS solutions. We also derive analytic NS solutions for $\sigma = \mathrm{const}$, $\sigma \propto \tau^{2/3}$, and $\sigma \propto 1/T^2$.

1. Solutions for ultrarelativistic gas with constant $2 \to 2$ cross section

For a *constant* cross section,

$$\lambda_{\mathrm{tr}}(\tau) \propto \tau \Rightarrow K(\tau) = \frac{\tau_0}{\lambda_{\mathrm{tr}}(\tau_0)} \equiv K_0 = \mathrm{const}. \tag{C2}$$

If we ignore the π_L^2 term, the *linear* equations of motion (35) and (36) can be solved in a straightforward manner:

$$\pi_L(\tilde{\tau}) = \tilde{\tau}^{-\frac{4}{3}-\frac{\kappa_0}{3}}\left[\frac{\pi_{L,0}}{2}T_+(\tilde{\tau}) - \frac{1}{2D}\left(\kappa_0\pi_{L,0} + \frac{8p_0}{3}\right)T_-(\tilde{\tau})\right], \tag{C3}$$

$$p(\tilde{\tau}) = \tilde{\tau}^{-\frac{4}{3}-\frac{\kappa_0}{3}}\left[\frac{p_0}{2}T_+(\tilde{\tau}) + \frac{1}{2D}(\kappa_0 p_0 - \pi_{L,0})T_-(\tilde{\tau})\right], \tag{C4}$$

where

$$\kappa_0 \equiv \frac{K_0}{C}, \quad D \equiv \sqrt{\frac{8}{3} + \kappa_0^2}, \quad T_\pm(x) \equiv x^{D/3} \pm x^{-D/3},$$
$$p(\tau_0) \equiv p_0, \quad \pi_L(\tau_0) \equiv \pi_{L,0}. \tag{C5}$$

For a practical approximate formula for the pressure evolution, see Eq. (48).

In the ideal hydrodynamic ($\eta_s \to 0$, or equivalently $\kappa_0 \to \infty$) limit, we recover

$$\pi_L(\tau > \tau_0) = 0, \quad p(\tau) = p_0\left(\frac{\tau_0}{\tau}\right)^{4/3}. \tag{C6}$$

At late times, the pressure anisotropy, regardless of its initial value $R_{p,0}$, approaches a *constant* determined solely by the parameter κ_0, i.e.,

$$R_\infty \equiv R_p(\tau \to \infty) = \frac{12\kappa_0 - 10}{9D + 3\kappa_0 + 14} < 1. \tag{C7}$$

For a finite κ_0, the final anisotropy is below unity.

Therefore, with a constant cross section, at late times the system does *not* behave like an ideal fluid, but instead the

Navier-Stokes limit applies [cf. Eqs. (44) and (45)]. Indeed, for large κ_0, Eqs. (C3)–(C4) reproduce the NS solution

$$p^{\rm NS}(\tau) = p_0 \left(\frac{\tau_0}{\tau}\right)^{4/3-4/(9\kappa_0)}, \quad \pi_L^{\rm NS}(\tau) = -\frac{4p^{\rm NS}(\tau)}{3\kappa_0}, \tag{C8}$$

and the final IS and NS anisotropies of Eqs. (C7) and (45) agree, that is, $R_\infty = 1 - 2/\kappa_0 + 4/(3\kappa_0^2) + \mathcal{O}(1/\kappa_0^3)$.

Because R_∞ is a monotonically increasing function of κ_0, the final pressure anisotropy is a measure of the viscosity. Inverting Eq. (C7),

$$\kappa_0 = \frac{5 + 14R_\infty - R_\infty^2}{6 - 3R_\infty - 3R_\infty^2}, \tag{C9}$$

i.e., near equilibrium ($\kappa_0 \gg 1$),

$$\begin{aligned} \frac{\eta_s(\tau)}{n(\tau)} = \frac{T\tau}{\kappa} &\approx \frac{1-R_\infty}{2} T_0\tau_0 \left(\frac{\tau}{\tau_0}\right)^\gamma, \\ \gamma &= \frac{2}{3} + \frac{4}{9}\frac{\eta_s(\tau_0)}{n_0}\frac{1}{T_0\tau_0}, \end{aligned} \tag{C10}$$

where in the last step we approximated the temperature evolution using the leading NS term (C8). It is natural to measure viscosity relative to the density, which up to a factor $(4-\chi)$ is the same as $\eta_s/s_{\rm eq}$.

The exact analytic solutions to the naive IS equations are analogous to Eqs. (C4) and (C3) but involve different powers of $\tilde\tau$

$$\tilde\tau^{\delta_\pm}, \quad \delta_\pm^{\rm naive} = -\frac{2}{3} - \frac{\kappa_0}{3} \pm \frac{\sqrt{\kappa_0^2 - 4\kappa_0 + \frac{20}{3}}}{3}. \tag{C11}$$

The late time behavior is governed by the exponent

$$\delta_+^{\rm naive} = -\frac{4}{3} + \frac{4}{9\kappa_0} + \frac{8}{9\kappa_0^2} + \mathcal{O}\left(\frac{1}{\kappa_0^3}\right), \tag{C12}$$

which does incorporate correctly the ideal hydrodynamic limit ($-4/3$) and the NS correction $4/(9\kappa_0)$ but is in general higher, the smaller the κ_0, than the complete IS result $\delta_+ = -4/3 + 4/(9\kappa_0) - 8/(27\kappa_0^3) + \mathcal{O}(1/\kappa_0^5)$. Therefore, the naive approach overestimates the pressure. In addition, it underestimates the asymptotic pressure anisotropy $R_\infty^{\rm naive} = 1 - 2/\kappa_0 - 8/(3\kappa_0^2) + \mathcal{O}(1/\kappa_0^3)$, and therefore, overpredicts the magnitude of the shear stress to pressure ratio $|\xi|$.

2. Solutions for ultrarelativistic gas with $\sigma_{2\to2} \propto 1/T^2$

A constant cross section implies the existence of some external scale in the problem. For a scale-invariant system, however, the only scale available (in thermal and chemical equilibrium) is the temperature, and therefore the cross section behaves as $\sigma \propto 1/T^2$. Equations (37), (33), and (29) then give

$$K(\tau) = K_0 \frac{T_0^2}{T^2} = \frac{K_0}{\tilde p^2 \tilde\tau^2}, \tag{C13}$$

i.e., even without the π_L^2 term, the equations of motion become nonlinear (but are easy to solve numerically).

For ideal hydrodynamic evolution, $p \propto \tau^{-4/3}$ and thus, unlike for the case of a constant cross section,

$$K(\tau) = K_0 \tilde\tau^{2/3} \tag{C14}$$

increases with increasing τ. $K(\tau)$ must grow in general in the viscous hydrodynamic case as well, because dissipative corrections, namely, the π_L/τ term in Eq. (35), are assumed to be small (or else hydrodynamics is no longer applicable). Consequently, the system gets *closer and closer* to ideal hydrodynamic behavior as time evolves (as long as the expansion is only one dimensional). For example, the pressure anisotropy approaches unity at late times, for *any* $\kappa_0 > 0$ and initial $\pi_{L,0}/p_0$,

$$R_p(\tau \to \infty) \to 1. \tag{C15}$$

The exact Navier-Stokes solution

$$p^{\rm NS}(\tau) = \left(\frac{\tau_0}{\tau}\right)^{4/3} \frac{p_0}{\sqrt{1 + \frac{4}{3\kappa_0}\left[\left(\frac{\tau_0}{\tau}\right)^{2/3} - 1\right]}} \tag{C16}$$

behaves similarly. At late times, $p \propto \tau^{-4/3}$ as in the ideal case, therefore, $\kappa(\tau\to\infty) = \kappa_0/(\tilde p^2\tilde\tau^2) \to \infty$, i.e., $R_\infty = 1$. The rate of approach to unity is controlled by the viscosity

$$\begin{aligned} R_p^{\rm NS}(\tau) &= 1 - \frac{2}{\kappa_0}\left(\frac{\tau_0}{\tau}\right)^{2/3}\left[1 + \mathcal{O}\left(1/\kappa_0^2\right) + \mathcal{O}((\tau_0/\tau)^{2/3})\right] \\ &\approx 1 - \frac{2}{T_0\tau_0}\frac{\eta_s}{n}\left(\frac{\tau_0}{\tau}\right)^{2/3}. \end{aligned} \tag{C17}$$

Viscosity also increases the pressure relative to the ideal case

$$\frac{p^{\rm NS}}{p_{\rm id}}(\tau \gg \tau_0) \to \frac{1}{\sqrt{1 - \frac{4}{3\kappa_0}}} \approx 1 + \frac{2}{3T_0\tau_0}\frac{\eta_s}{n}. \tag{C18}$$

3. Solutions for ultrarelativistic gas with $\sigma_{2\to2} \propto \tau^{2/3}$

Near the ideal hydrodynamic limit (i.e., for small viscosities and $\pi_{L,0}/p_0$), one may directly substitute the approximate result (C14) in the equations of motion (35) and (36). Provided we drop the π_L^2 term, these can be converted to a second-order linear differential equation, e.g., for $p(\tau)$,

$$\tau\ddot p + \frac{11}{3}\dot p + \frac{40}{27}\frac{p}{\tau} + \frac{2K(\tau)}{3C}\left(\dot p + \frac{4}{3}\frac{p}{\tau}\right) = 0, \tag{C19}$$

with initial conditions

$$p(\tau_0) = p_0, \quad \dot p(\tau_0) = -\frac{4p_0 + \pi_{L,0}}{3\tau_0}. \tag{C20}$$

The general solution with $K(\tau)$ from Eq. (C14) is[9]

$$p(\tilde\tau) = \tilde\tau^{-4/3}\left[C_-\tilde\tau^{-\frac{2\sqrt6}{9}}F_-(\kappa_0\tilde\tau^{2/3}) + C_+\tilde\tau^{\frac{2\sqrt6}{9}}F_+(\kappa_0\tilde\tau^{2/3})\right], \tag{C21}$$

$$\pi_L(\tilde\tau) = -3\,\tilde\tau^{-1/3}\frac{d[\tilde\tau^{4/3}p(\tilde\tau)]}{d\tilde\tau}, \tag{C22}$$

[9]First substitute $p(\tilde\tau) \equiv \bar p(\tilde\tau)\tilde\tau^{-4/3}$, then switch to a new variable $x \equiv -\kappa_0\tilde\tau^{2/3}$, finally look for the solution in the form $\bar p(x) \equiv x^a q(x)$, and choose a suitable a.

where

$$F_\pm(x) \equiv {}_1F_1(\pm a, 1 \pm 2a; -x), \quad a = \sqrt{\frac{2}{3}} \tag{C23}$$

are short-hand for confluent hypergeometric functions of the first kind, while $C_\pm$ are matched[10] to the initial conditions in Eq. (C20):

$$C_\pm = \pm\frac{e^{\kappa_0}}{4a}[p_0 G_\mp(\kappa_0) - \pi_{L,0} F_\mp(\kappa_0)], \tag{C24}$$

$$G_\pm(x) \equiv \pm 2a\left[\frac{x}{1 \pm 2a}\,{}_1F_1(1 \pm a, 2 \pm 2a, -x) - {}_1F_1(\pm a, 1 \pm 2a, -x)\right]. \tag{C25}$$

A very practical approximate formula for the pressure evolution is given by Eq. (49), which comes from the asymptotic forms [cf. Eq. (13.5.1) in Ref. [42]]

$${}_1F_1(a, b; -x) = \frac{\Gamma(b)}{\Gamma(b-a)} x^{-a} S(a, 1 + a - b, x) + \frac{\Gamma(b)}{\Gamma(a)} e^{-x}(-x)^{a-b} S(b - a, 1 - a, -x), \tag{C26}$$

where

$$S(c, d, x) \equiv 1 + \frac{c\,d}{1!x} + \frac{c(c+1)d(d+1)}{2!\,x^2} + \frac{c(c+1)(c+2)d(d+1)(d+2)}{3!\,x^3} + \cdots \tag{C27}$$

Note that the e^{-x} term in Eq. (C26) is crucial. For large κ_0, $C_\pm$ are exponentially large; however, the e^{κ_0} factors drop out[11] in linear combinations relevant for the pressure and shear stress.

At late times $\tau \gg \tau_0/\kappa_0^{3/2}$, the IS solutions recover ideal hydrodynamics for any initial condition,

$$p(\tau) \propto \left(\frac{\tau_0}{\tau}\right)^{4/3}, \quad \pi_L(\tau) \propto \left(\frac{\tau_0}{\tau}\right)^2 \Rightarrow \frac{\pi_L}{p}(\tau) \propto \left(\frac{\tau_0}{\tau}\right)^{2/3} \to 0, \quad \text{for} \quad \tau \gg \frac{\tau_0}{\kappa_0^{3/2}}, \tag{C28}$$

as can be inferred from Eq. (C26). The NS solution

$$p^{\rm NS}(\tau) = p_0 \left(\frac{\tau_0}{\tau}\right)^{4/3} \exp\left\{\frac{2}{3\kappa_0}\left[1 - \left(\frac{\tau_0}{\tau}\right)^{2/3}\right]\right\} \tag{C29}$$

exhibits the same features (as the reader can easily verify). For the late-time evolution, this scenario gives smaller viscous corrections to the pressure and the pressure anisotropy than $\sigma \propto 1/T^2$. However, in the large κ_0 limit, we recover the same results in Eqs. (C17) and (C18).

Analogous derivation gives the exact solutions in the naive IS case:

$$p(\tilde\tau) = C'_-\tilde\tau^{-2(1+a')/3} F'_-(\kappa_0\tilde\tau^{2/3}) + C'_+\tilde\tau^{-2(1-a')/3} F'_+(\kappa_0\tilde\tau^{2/3}), \tag{C30}$$

$$a' = \sqrt{\frac{5}{3}},$$

$$\pi_L(\tilde\tau) = -3\tilde\tau^{-1/3}\frac{d[\tilde\tau^{4/3}p(\tilde\tau)]}{d\tilde\tau}, \tag{C31}$$

where

$$C'_\pm = \pm\frac{e^{-\kappa_0}}{4a'}[p_0 G'_\mp(\kappa_0) - \xi_0 F'_\mp(\kappa_0)], \tag{C32}$$

$$F'_\pm(x) \equiv {}_1F_1(1 \pm a', 1 \pm 2a', -x), \tag{C33}$$

$$G'_\pm(x) \equiv 2x\frac{1 \pm a'}{1 \pm 2a'}F'_\pm(x) - 2(1 \pm a')F'_\pm(x). \tag{C34}$$

With the help of Eq. (C26), it is straightforward (but somewhat lengthy) to determine the late-time behavior

$$\frac{p}{p_{\rm id}} = T(\tilde\tau)[P(\kappa_0) + \xi_0 X(\kappa_0)], \tag{C35}$$

where in the naive case,

$$T^{\rm naive}(\tilde\tau) = 1 - \frac{2}{3\kappa_0\tilde\tau^{2/3}} - \frac{7}{9\kappa_0^2\tilde\tau^{4/3}} + \mathcal{O}\left(\frac{1}{\kappa_0^3\tilde\tau^2}\right), \tag{C36}$$

$$P^{\rm naive}(\kappa_0) = 1 + \frac{2}{3\kappa_0} + \frac{5}{9\kappa_0^2} + \mathcal{O}\left(\frac{1}{\kappa_0^3}\right), \tag{C37}$$

$$X^{\rm naive}(\kappa_0) = -\frac{1}{2\kappa_0} - \frac{5}{6\kappa_0^2} + \mathcal{O}\left(\frac{1}{\kappa_0^3}\right). \tag{C38}$$

Comparing to the complete Israel-Stewart result of Eq. (C21) (obtained in the small ξ limit),

$$T^{\rm IS}(\tilde\tau) \approx 1 - \frac{2}{3\kappa_0\tilde\tau^{2/3}} - \frac{1}{9\kappa_0^2\tilde\tau^{4/3}} + \mathcal{O}\left(\frac{1}{\kappa_0^3\tilde\tau^2}\right), \tag{C39}$$

$$P^{\rm IS}(\kappa_0) \approx 1 + \frac{2}{3\kappa_0} - \frac{1}{9\kappa_0^2} + \mathcal{O}\left(\frac{1}{\kappa_0^3}\right), \tag{C40}$$

$$X^{\rm IS}(\kappa_0) \approx -\frac{1}{2\kappa_0} + \frac{1}{6\kappa_0^2} + \mathcal{O}\left(\frac{1}{\kappa_0^3}\right), \tag{C41}$$

we see that for the naive approximation, the evolution approaches ideal hydrodynamic $p/p_{\rm id} \sim$ const behavior *later*

[10] Note that

$$\frac{d}{dx}{}_1F_1(a, b, x) \equiv \frac{a}{b}{}_1F_1(a + 1, b + 1, x),$$

and from the Wronskian,

$$G_-(x)F_+(x) - G_+(x)F_-(x) = 4a\,e^{-x}$$

[cf. $W\{1, 2\}$ in Eq. (13.1.20) in Ref. [42]].

[11] For example,

$$\frac{\Gamma(1+2a)}{\Gamma(1+a)}F_-(\kappa_0)\kappa_0^{-a} - \frac{\Gamma(1-2a)}{\Gamma(1-a)}F_+(\kappa_0)\kappa_0^a = 2a\frac{e^{-\kappa_0}}{\kappa_0}\left[1 - \frac{1}{3\kappa_0} + \mathcal{O}\left(\frac{1}{\kappa_0^2}\right)\right]$$

and

$$\frac{\Gamma(1+2a)}{\Gamma(1+a)}G_-(\kappa_0)\kappa_0^{-a} - \frac{\Gamma(1-2a)}{\Gamma(1-a)}G_+(\kappa_0)\kappa_0^a = 4ae^{-\kappa_0}\left[1 + \frac{2}{3\kappa_0} - \frac{1}{9\kappa_0^2} + \mathcal{O}\left(\frac{1}{\kappa_0^3}\right)\right]$$

($a = \sqrt{2/3}$).

(deviation of T from unity is larger), and for near-equilibrium initial conditions ($\xi_0 \approx 0$), the pressure saturates at a *higher* value (P is larger).

4. Solutions for ultrarelativistic gas with $2 \to 2$ cross section and $\eta_s/s_{\rm eq} = {\rm const}$

The last scenario we consider is when the cross section is dynamically adjusted to maintain a *constant* shear viscosity to equilibrium entropy density ratio $\eta_s/s_{\rm eq}$, such as the conjectured lower bound of $1/(4\pi)$. From Eqs. (29), (33), (51), and (52),

$$\tilde{s}_{\rm eq} = \frac{1}{\tilde{\tau}}\left(1 + \frac{\ln[\tilde{\tau}^4\tilde{p}^3(\tilde{\tau})]}{4-\chi_0}\right), \tag{C42}$$

and thus

$$\frac{\eta_s}{s_{\rm eq}} = \frac{\eta_{s,0}}{s_{eq,0}}\frac{\tilde{p}(\tilde{\tau})\tilde{\tau}^2}{\tilde{K}(\tilde{\tau})}\frac{4-\chi_0}{4-\chi_0+\ln[\tilde{\tau}^4\tilde{p}^3(\tilde{\tau})]}, \tag{C43}$$

where

$$\frac{\eta_{s,0}}{s_{eq,0}} = \frac{T_0\tau_0}{\kappa_0(4-\chi_0)}. \tag{C44}$$

Therefore, $\eta_s/s_{\rm eq} = {\rm const}$ requires

$$K(\tilde{\tau}) = K_0\tilde{p}(\tilde{\tau})\tilde{\tau}^2\frac{4-\chi_0}{4-\chi_0+\ln[\tilde{\tau}^4\tilde{p}^3(\tilde{\tau})]}. \tag{C45}$$

Within the generic region of validity for viscous hydrodynamics, $|\pi_L| \ll p$, this scenario also implies a growing $K(\tau) \sim \tau^{\approx 2/3}$ and therefore convergence to the ideal limit at late times. Note that the double ratio $(\eta_s/s_{\rm eq})/(\eta_{s,0}/s_{eq,0})$ as a function of τ/τ_0 depends only on $\pi_{L,0}/p_0$, κ_0, the type of cross section (encoded in $\tilde{K}$), and χ_0.

We now analyze the time evolution of $\eta_s/s_{\rm eq}$ in the three earlier scenarios. Compared to the entropy density, $\eta_s/s_{\rm eq}$ contains an additional multiplicative term that comes from the time evolution of the shear viscosity. Assume first, for simplicity, that we are very close to the ideal hydrodynamic limit, in which case, $\eta_s/s_{\rm eq} \propto \tau^{2/3}/K(\tau)$. For a constant cross section, this results in a *growing* $\eta_s/s_{\rm eq} \propto \tau^{2/3}$; while for the other two cases, $\sigma \propto \tau^{2/3}$ or $\sigma \propto 1/T^2$, we obtain $\eta_s/s_{\rm eq} \approx$ const.

In reality, there are of course viscous effects. Because

$$\frac{\tilde{p}(\tilde{\tau})\tilde{\tau}^2}{\tilde{K}(\tilde{\tau})} = \begin{cases} \tilde{p}(\tilde{\tau})\tilde{\tau}^{4/3} \times \tilde{\tau}^{2/3} & \text{for} \quad \sigma = \text{const}, \\ [\tilde{p}(\tilde{\tau})\tilde{\tau}^{4/3}]^3 & \text{for} \quad \sigma \propto 1/T^2, \\ \tilde{p}(\tilde{\tau})\tilde{\tau}^{4/3} & \text{for} \quad \sigma \propto \tau^{2/3}, \end{cases} \tag{C46}$$

the relevant quantity that determines the evolution of $\eta_s/s_{\rm eq}$ is $\tilde{p}\tilde{\tau}^{4/3}$. The last term in Eq. (C43) is only a logarithm. Therefore, the first term, Eq. (C46), dominates the behavior. Typically, $\pi_L < 0$ and thus dissipation generates an increasing $\tilde{p}\tilde{\tau}^{4/3}$. The increase in $\eta_s/s_{\rm eq}$ is then fastest for the constant cross section case. The other two cases, $\sigma \propto 1/T^2$ and $\sigma \propto \tau^{2/3}$, are not equivalent when there is dissipation, because for the latter the prefactor in Eq. (C46) is only linear in $\tilde{p}(\tilde{\tau})\tilde{\tau}^{4/3}$ and, therefore, $\eta_s/s_{\rm eq}$ grows much slower.

5. Comparison of the various cross section scenarios

After exploring the general behavior, we compare numerical solutions for the four scenarios. Unless stated otherwise, for the $\eta_s/s_{\rm eq} = {\rm const}$ case, we start the evolution from chemical equilibrium, i.e., take $\chi_0 = 0$. For the other three scenarios, the pressure and shear stress evolution does not depend on χ_0. For simplicity, we start the evolution from $\pi_L(\tau_0) = 0$, and consider two extremes $K_0 = 1$, i.e., equal expansion and scattering time scales, and $K_0 = 6.67$, i.e., 6.67 times slower expansion than the time scale for scattering. On all figures, the dotted curves correspond to the approximation when the π_L^2 term in Eq. (36) is ignored.

Figure 8 shows the evolution of the pressure relative to the ideal hydrodynamic $p \sim \tau^{-4/3}$ result (for a comparison of the same observable between hydrodynamics and transport, see Fig. 4). Dissipation increases the pressure because it reduces the pdV work. The effect is largest for the $\sigma = {\rm const}$ scenario, while it is smallest for $\eta_s/s_{\rm eq} = {\rm const}$ and $\sigma \propto \tau^{2/3}$, which two scenarios give basically the same result. For $K_0 = 1$, the fourth scenario $\sigma \propto 1/T^2$ is in between these limits; but by $K_0 = 6.67$, it becomes equivalent to $\sigma \propto \tau^{2/3}$. Dropping the π_L^2 terms in Eq. (36) (thin dotted lines) is a fair 10–15% approximation for $\sigma = {\rm const}$ and $\sigma \propto 1/T^2$ at $K_0 = 1$, which improves to an essentially exact one by $K_0 = 6.67$. For the other two scenarios, $\eta_s/s_{\rm eq} = {\rm const}$ and $\sigma \propto \tau^{2/3}$, the nonlinear term can be safely ignored already for $K_0 = 1$. Note that for $K_0 = 6.67$, dissipative corrections to the pressure are still very modest 10–15% at late $\tau/\tau_0 \sim$ 10–20 in all four cases studied.

Now we turn to the evolution of the viscous stress π_L shown in Fig. 9. All four scenarios give very similar results for the early $\tau/\tau_0 \lesssim 1.5$–2 growth in magnitude, but they differ in late-time relaxation. As inferred from the pressure evolution already, $\eta_s/s_{\rm eq} = {\rm const}$ and $\sigma \propto \tau^{2/3}$ are largely identical and relax quickly toward the ideal limit. $\sigma = {\rm const}$ is the one that stays farthest from equilibrium. For low $K_0 = 1$, the $\sigma \propto 1/T^2$ case lies in between; but by $K_0 = 6.67$, it becomes identical to $\eta_s/s_{\rm eq} = {\rm const}$ and $\sigma \propto \tau^{2/3}$. The π_L^2 term in the equation

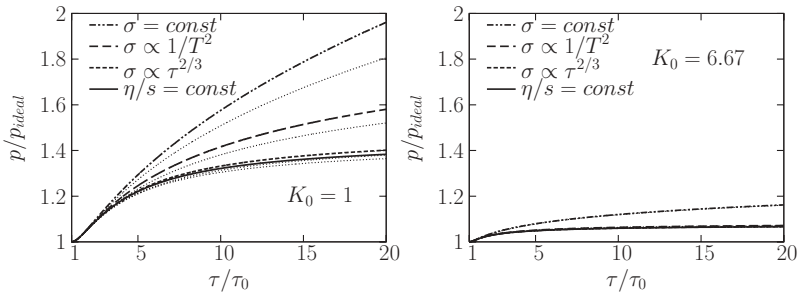

FIG. 8. Pressure evolution from viscous hydrodynamics relative to the ideal hydrodynamic $p = p_0(\tau_0/\tau)^{-4/3}$ result in 0 + 1D Bjorken geometry for an ultrarelativistic gas with $2 \to 2$ interactions. Four scenarios are compared for $K_0 = 1$ and 6.67: $\sigma = {\rm const}$, $\sigma \propto 1/T^2$, $\sigma \propto \tau^{2/3}$, and $\eta_s/s_{\rm eq} = {\rm const}$. Approximate results with dropping π_L^2 terms in the equation of motion are also shown (thin dotted lines).

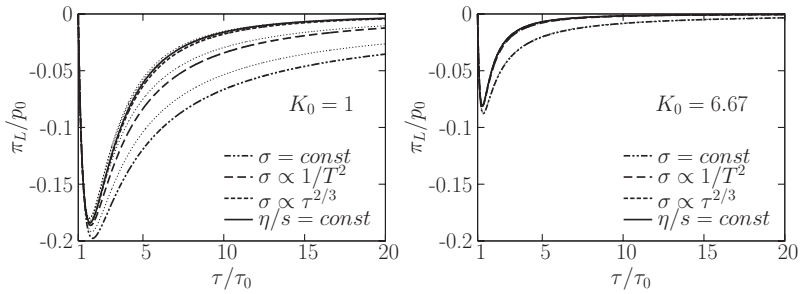

FIG. 9. Same as Fig. 8, but for the longitudinal viscous shear π_L normalized by the *initial* pressure.

of motion affects the pressure and the viscous stress similarly and can be ignored for $K_0 = 6.67$ in all cases and for $\sigma \propto \tau^{2/3}$ and $\eta_s/s_{\rm eq} = \text{const}$ even at $K_0 = 1$.

The same observations carry over to the pressure anisotropy $R_p = p_L/p_T$ shown in Fig. 10. We plot this quantity because it is the same one shown in Fig. 1 for the hydrodynamics vs. transport theory comparison in Sec. V (but note the logarithmic time axis there). These results further confirm that $\sigma \propto \tau^{2/3}$ is a very good approximation to $\eta_s/s_{\rm eq} = \text{const}$ already for $K_0 = 1$.

Figure 11 shows entropy production $dS/d\eta$ as a function of proper time for the four scenarios, with local thermal ($\xi_0 = 0$) and chemical ($\chi_0 = 0$) equilibrium initial conditions. Due to scalings, only entropy relative to the initial one plays a role, i.e.,

$$\frac{(dS/d\eta)}{(dS_0/d\eta)} = \tilde{\tau}\tilde{s} = 1 + \frac{1}{4-\chi_0}\left[\ln(\tilde{\tau}^4\tilde{p}^3) - \frac{9\xi^2(\tau)}{16}\right]. \quad \text{(C47)}$$

For $K_0 = 1$, a constant cross section generates about 35% extra entropy by late $\tau \sim (15\text{–}20)\tau_0$. With $\sigma \propto 1/T^2$, the increase is only ∼30%; whereas $\sigma \propto \tau^{2/3}$ and $\eta_s/s_{\rm eq} = \text{const}$ give the smallest increase of about 25%. For a larger $K_0 \sim 7$, the system is much closer to ideal hydrodynamics and therefore entropy generation is slower, about 10% for $\sigma = \text{const}$, while only 5% for the other three cases. Note that these results also depend on χ_0 but almost entirely through the explicit $1/(4-\chi_0)$ factor in Eq. (C47). Therefore, results for arbitrary $\chi_0 \neq 0$ can be obtained via straightforward rescaling. In the $\eta_s/s_{\rm eq} = \text{const}$ case, the shear stress and pressure evolution also depend on χ_0 but only very weakly, as we show later below (cf. Fig. 13).

Figure 12 shows the evolution of the shear viscosity to equilibrium entropy density ratio $\eta_s/s_{\rm eq}$, normalized by the initial value of the ratio. The entropy is calculated for a system starting from chemical equilibrium ($\chi_0 = 0$). The rough expectations that $\eta_s/s_{\rm eq} \sim \tau^{2/3}$ for a constant cross section, while $\eta_s/s_{\rm eq} \sim \text{const}$ for both $\sigma \propto 1/T^2$ and $\sigma \propto \tau^{2/3}$, hold within a factor of 3 already for $K_0 = 1$ and up to $\tau = 20\tau_0$ (note that the $\tau^{2/3}$ growth in the $\sigma = \text{const}$ case has been scaled out in the plots). Relative to this zeroth-order behavior, for all three scenarios, $\eta_s/s_{\rm eq}$ grows with time, reinforcing the general results in Sec. C4. The relative growth decreases with increasing K_0. The K_0 dependence is strongest for the constant cross section scenario: the factor of 3 gain by $\tau = 20\tau_0$ for $K_0 = 1$ is tamed to about a 25% increase for $K_0 \sim 7$. For the other two scenarios, $\sigma \propto 1/T^2$ and $\sigma \propto \tau^{2/3}$, the ratio stays nearly constant much more robustly. As expected (cf. end of Appendix C 4), of all cases studied, $\sigma \propto \tau^{2/3}$ approximates $\eta_s/s_{\rm eq} = \text{const}$ the best, with only ∼10% deviation accumulated by late $\tau = 20\tau_0$ even for a small $K_0 = 1$.

Finally, in Fig. 13, we show that the results for $\eta_s/s_{\rm eq} = \text{const}$ depend only weakly on the initial density, i.e., χ_0. Density dependence in shear stress and pressure evolution arises in this case because the cross section is a function of the initial density [see Eq. (C45)]. The dependence is weaker the closer the system is to ideal hydrodynamics, because in that case $p \propto \tau^{-4/3}$ and χ_0 drops out from $K(\tau)$. But even for a pessimistic $K_0 = 1$, the pressure anisotropy $R_p = p_L/p_T$, varies less than 10% as we change the density by a factor of 4 around chemical equilibrium density ($\chi_0 = \pm \ln 4$). In fact, a decrease in the density has a much weaker effect than an increase. The right plot shows the effect of the same initial density variation on entropy $dS/d\eta$ production normalized to the initial entropy. Most of the density dependence in the entropy change comes from the trivial $1/(4-\chi_0)$ prefactor in Eq. (C47), which is there in any cross section scenario even if the shear stress and pressure evolution are independent of the density. To highlight dynamical density effects, we therefore plot, again for a pessimistic $K_0 = 1$, the normalized change in entropy

$$\frac{4-\chi_0}{4}\frac{\Delta(dS/d\eta)}{(dS_0/d\eta)} \equiv \frac{4-\chi_0}{4}\left(\frac{(dS/d\eta)}{(dS_0/d\eta)} - 1\right). \quad \text{(C48)}$$

(The scaling factor is chosen such that it has no effect for chemical equilibrium initial conditions $\chi_0 = 0$.) The results show practically no density dependence, apart from few-percent changes, even for such a low K_0.

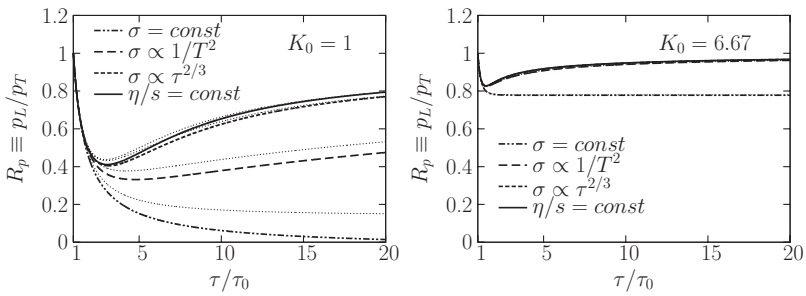

FIG. 10. Same as Fig. 8, but for the pressure anisotropy evolution.

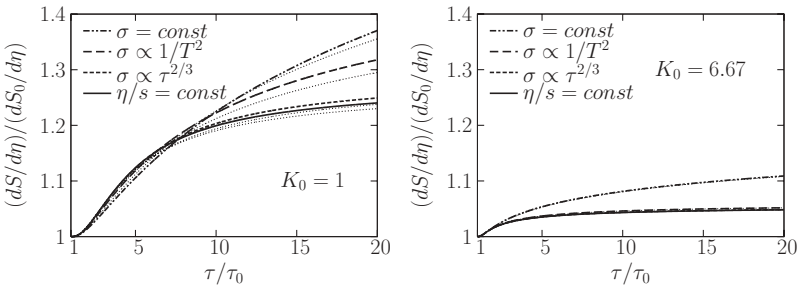

FIG. 11. Same as Fig. 8, but for the normalized entropy per unit rapidity $(dS/d\eta)/(dS_0/d\eta)$.

APPENDIX D: USEFUL RELATIONS FROM COVARIANT TRANSPORT

1. Particle number and transverse energy

The particle number and transverse energy distributions for particles crossing a three-dimensional hypersurface $\sigma(x) =$ const are given by

$$dN = dy\, dp_T^2 \int p^\mu d\sigma_\mu(x) f(x, \mathbf{p}), \tag{D1}$$

$$dE_T = dy\, dp_T^2 \int p^\mu d\sigma_\mu(x) m_T f(x, \mathbf{p}), \tag{D2}$$

where $m_T \equiv \sqrt{p_T^2 + m^2}$, $p_T \equiv \sqrt{p_x^2 + p_y^2}$ is the transverse momentum, and $d\sigma_\mu(x)$ is the normal to the hypersurface at space-time coordinate x. For our boost-invariant scenario, it is natural to follow quantities per *unit coordinate rapidity* as a function of the proper time τ. For $\tau =$ const, hypersurfaces $p^\mu d\sigma_\mu = m_T \tau \operatorname{ch}\omega\, d^2x_T\, d\eta$, and in our 0 + 1D case, f only depends on $\operatorname{sh}\omega$, $p_\perp$, and τ, where $\omega \equiv y - \eta$. Thus,

$$\frac{dN(\tau)}{d\eta} = \tau A_T \int d^2p_T\, d\omega\, m_T \operatorname{ch}\omega\, f(\tau, \operatorname{sh}\omega, p_T), \tag{D3}$$

$$\frac{dE_T(\tau)}{d\eta} = \tau A_T \int d^2p_T\, d\omega\, m_T^2 \operatorname{ch}\omega\, f(\tau, \operatorname{sh}\omega, p_T), \tag{D4}$$

A_T is the transverse area of the system. With the local thermal equilibrium distribution for ultrarelativistic particles

$$f(\operatorname{sh}\omega, p_\perp) = \mathcal{N} e^{-p_\perp \operatorname{ch}\omega/T}, \quad \mathcal{N} = \frac{n}{8\pi T^3}, \tag{D5}$$

and the quadratic form (62), straightforward integration gives

$$\frac{dN}{d\eta} = n\,\tau A_T = \text{const}, \tag{D6}$$

$$\frac{dE_T(\tau)}{d\eta} = \frac{3\pi T}{4}\frac{dN}{d\eta}\left(1 - \frac{5\xi}{16}\right). \tag{D7}$$

Clearly, dissipation slows the decrease of transverse energy (for typical $\pi_L < 0$), and $2 \to 2$ interactions, of course, conserve the particle number.

Note that $dE_T/d\eta/(\tau A_T)$ is almost identical to the transverse pressure of Eq. (D10) but has an extra $\operatorname{ch}\omega$ factor in the integrand.

2. Early pressure evolution

Here we evaluate the early transverse and longitudinal pressure evolution from the transport for a local equilibrium initial condition. The results hold for *any* interaction, not only $2 \to 2$.

In local equilibrium, the collision term vanishes; thus in the vicinity of $\tau = \tau_0$, the evolution is governed by *free streaming*.[12] In our 0 + 1D case, free streaming

$$\left[\operatorname{ch}\omega\, \partial_\tau - \frac{\operatorname{sh}\omega}{\tau}\partial_\omega\right] f(\operatorname{sh}\omega, p_\perp, \tau) = 0 \quad (\omega \equiv y - \eta) \tag{D8}$$

implies

$$f(\operatorname{sh}\omega, p_\perp, \tau) = f(\tau \operatorname{sh}\omega/\tau_0, p_\perp, \tau_0). \tag{D9}$$

[12]The approach followed here is equivalent to a direct computation of the coefficient $\dot{R}_0$ in the Taylor expansion $R(\tau) = 1 + \dot{R}_0(\tau - \tau_0) + \ddot{R}_0(\tau - \tau_0)^2/2 + \cdots$. In the direct approach, one would differentiate Eq. (43) to obtain

$$\dot{R}_0 = \frac{\dot{T}_{zz}(\tau_0) - \dot{T}_{xx}(\tau_0)}{p_0},$$

then substitute T_{zz} and T_{xx} from Eq. (D10), and replace $\dot{f}(\operatorname{ch}\omega, p_\perp, \tau_0)$ with $\partial_\omega f(\operatorname{ch}\omega, p_\perp, \tau_0)$ using the Boltzmann equation. For locally equilibrated initial conditions of Eq. (D5), the collision term vanishes, and the problem is then reduced to straightforward integration, which yields $\dot{R}_0 = -8/(5\tau_0)$.

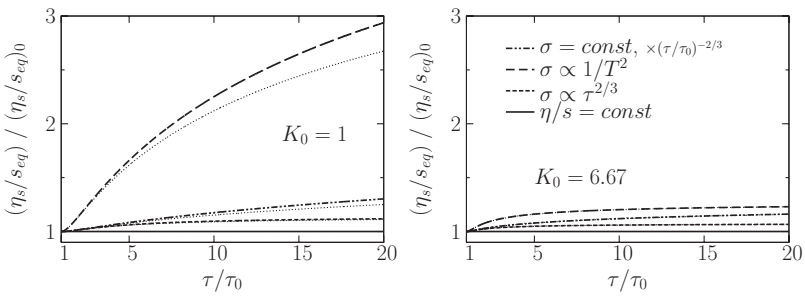

FIG. 12. Same as Fig. 8, but for the shear viscosity to equilibrium entropy density ratio $\eta_s/s_{\rm eq}$. The results for $\sigma =$ const are divided by $(\tau/\tau_0)^{2/3}$, otherwise they would quickly grow off the plot.

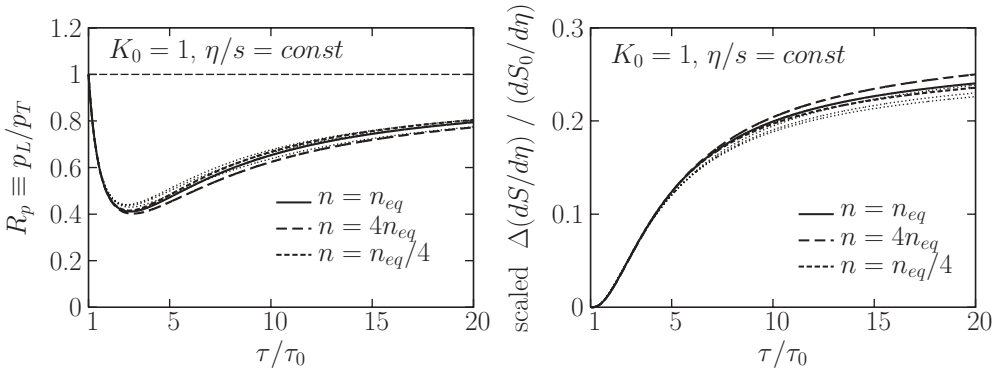

FIG. 13. Initial density dependence of Israel-Stewart viscous hydrodynamic solutions for an ultrarelativistic gas expanding longitudinally in 0 + 1D Bjorken geometry with $2 \to 2$ interactions that maintain $\eta_s/s_{\rm eq} = \text{const}$. To amplify density effects, the initial expansion time scale to mean free path ratio is chosen to be low, $K_0 = 1$. Three different *initial* densities are considered: chemical equilibrium $n = n_{\rm eq}$, oversaturation at $n = 4n_{\rm eq}$, and undersaturation at $n = n_{\rm eq}/4$. Left: time evolution of the pressure anisotropy $R_p = p_L/p_T$. Right: time evolution of the *produced* entropy per unit rapidity, normalized to the initial entropy per unit rapidity. The produced entropy is scaled by $(4 - \chi_0)/4$ to eliminate trivial density effects that do not come from the shear stress and pressure evolution (see text). Approximate results with dropping π_L^2 terms in the equation of motion are also shown (thin dotted lines).

Substituting a local thermal initial distribution for ultrarelativistic particles [Eq. (D5)], the definition of the energy-momentum tensor

$$T^{\mu\nu}(\eta = 0, \tau) = \int \frac{d^3p}{p_0} p^\mu p^\nu f$$

$$= \int d^2p_\perp dy p^\mu p^\nu f(\text{sh}y, p_\perp, \tau) \quad \text{(D10)}$$

gives the transverse pressure

$$p_T(\tau) \equiv T^{xx}(\eta = 0, \tau) = \mathcal{N} \int dp_\perp p_\perp d\phi dy (p_\perp \cos\phi)^2$$

$$\times \exp\left[-\frac{p_\perp}{T_0}\sqrt{1 + a^2\text{sh}^2 y}\right]$$

$$= \frac{3T_0 n}{2} \int_0^\infty \frac{dy}{(1 + a^2\text{sh}^2 y)^2}. \quad \text{(D11)}$$

Here $a \equiv \tau/\tau_0$. Change of variables to $q = a\,\text{sh}\,y$ leads to

$$p_T(\tau) = \frac{3T_0 n}{2} \int_0^\infty \frac{dq}{(1 + q^2)^2\sqrt{q^2 + a^2}}$$

$$= T_0 n\, \frac{3\left[\sqrt{a^2 - 1} + (a^2 - 2)\text{acos}\frac{1}{a}\right]}{4(a^2 - 1)^{3/2}}. \quad \text{(D12)}$$

Analogous calculation gives for the longitudinal pressure,

$$p_L(\tau) \equiv T^{zz}(\eta = 0, \tau) = 3T_0 n \int \frac{dy\,\text{sh}^2 y}{(1 + a^2\text{sh}^2 y)^2}$$

$$= T_0 n \frac{3}{2(a^2 - 1)}\left[\frac{\text{acos}\frac{1}{a}}{\sqrt{a^2 - 1}} - \frac{1}{a^2}\right]. \quad \text{(D13)}$$

Expanding near $a = 1$,

$$p_T(\tau) = T_0 n \left[1 - \frac{4(\tau - \tau_0)}{5\tau_0} + \mathcal{O}((\tau - \tau_0)^2)\right], \quad \text{(D14)}$$

$$p_L(\tau) = T_0 n \left[1 - \frac{12(\tau - \tau_0)}{5\tau_0} + \mathcal{O}((\tau - \tau_0)^2)\right], \quad \text{(D15)}$$

and thus Eq. (65) follows.

[1] P. Danielewicz and M. Gyulassy, Phys. Rev. D **31**, 53 (1985).
[2] G. Policastro, D. T. Son, and A. O. Starinets, Phys. Rev. Lett. **87**, 081601 (2001); P. K. Kovtun, D. T. Son, and A. O. Starinets, *ibid.* **94**, 111601 (2005).
[3] M. Brigante, H. Liu, R. C. Myers, S. Shenker, and S. Yaida, Phys. Rev. Lett. **100**, 191601 (2008).
[4] P. F. Kolb and U. W. Heinz, arXiv:nucl-th/0305084.
[5] M. Gyulassy and L. McLerran, Nucl. Phys. **A750**, 30 (2005).
[6] E. V. Shuryak, Nucl. Phys. **A750**, 64 (2005).
[7] H. Stoecker, Nucl. Phys. **A750**, 121 (2005).
[8] D. Molnar and P. Huovinen, Phys. Rev. Lett. **94**, 012302 (2005).
[9] A. Muronga, Phys. Rev. Lett. **88**, 062302 (2002); **89**, 159901(E) (2002).
[10] D. A. Teaney, J. Phys. G **30**, S1247 (2004).
[11] R. Baier, P. Romatschke, and U. A. Wiedemann, Nucl. Phys. **A782**, 313 (2007).
[12] U. W. Heinz, H. Song, and A. K. Chaudhuri, Phys. Rev. C **73**, 034904 (2006).
[13] P. Romatschke, Eur. Phys. J. C **52**, 203 (2007).
[14] T. Koide, G. S. Denicol, Ph. Mota, and T. Kodama, Phys. Rev. C **75**, 034909 (2007).
[15] P. Romatschke and U. Romatschke, Phys. Rev. Lett. **99**, 172301 (2007).
[16] H. Song and U. W. Heinz, Phys. Lett. **B658**, 279 (2008).
[17] K. Dusling and D. Teaney, Phys. Rev. C **77**, 034905 (2008).
[18] D. Molnar and P. Huovinen, J. Phys. G **35**, 104125 (2008).

[19] W. A. Hiscock and L. Lindblom, Phys. Rev. D **31**, 725 (1985).
[20] E. M. Lifshitz and L. D. Landau, *Fluid Mechanics* (Butterworth-Heinemann, Oxford, 1987).
[21] S. R. de Groot, W. A. van Leeuwen, and Ch. G. van Weert, *Relativistic Kinetic Theory—Principles and Applications* (North-Holland, Amsterdam, 1980).
[22] W. Israel, Ann. Phys. (NY) **100**, 310 (1976).
[23] W. Israel and J. M. Stewart, Ann. Phys. (NY) **118**, 349 (1979).
[24] See Chapter V of Ref. [21].
[25] L. Lindblom, Ann. Phys. (NY) **247**, 1 (1996); P. Geroch, J. Math. Phys. **36**, 4226 (1995).
[26] B. Zhang, Comput. Phys. Commun. **109**, 193 (1998).
[27] M. Gyulassy, Y. Pang, and B. Zhang, Nucl. Phys. **A626**, 999 (1997).
[28] D. Molnar and M. Gyulassy, Phys. Rev. C **62**, 054907 (2000).
[29] D. Molnar and M. Gyulassy, Nucl. Phys. **A697**, 495 (2002); **A703**, 893(E) (2002); **A698**, 379 (2002).
[30] J. D. Bjorken, Phys. Rev. D **27**, 140 (1983).
[31] D. Molnar, arXiv:0806.0026.
[32] I. Müller, Z. Phys. **198**, 329 (1967).
[33] See Chapter VI of Ref. [21].
[34] R. Baier, P. Romatschke, and U. A. Wiedemann, Phys. Rev. C **73**, 064903 (2006).
[35] H. Song and U. W. Heinz, Phys. Rev. C **78**, 024902 (2008).
[36] P. Huovinen, Eur. Phys. J. A **37**, 121 (2008).
[37] J. Manninen and F. Becattini, Phys. Rev. C **78**, 054901 (2008).
[38] A. Dumitru, E. Molnar, and Y. Nara, Phys. Rev. C **76**, 024910 (2007).
[39] D. Molnar, MPC 1.8.5 transport code, http://karman.physics.purdue.edu/OSCAR.
[40] D. Kharzeev and K. Tuchin, J. High Energy Phys. 09 (2008) 093; F. Karsch, D. Kharzeev, and K. Tuchin, Phys. Lett. **B663**, 217 (2008).
[41] R. J. Fries, B. Muller, and A. Schafer, Phys. Rev. C **78**, 034913 (2008).
[42] M. Abramowitz and I. A. Stegun, *Handbook of Mathematical Functions* (Dover, New York, 1972).